Second Generation Drosophila Chemical Tags: Sensitivity, Versatility and Speed

December 19, 2016

Ben Sutcliffe[1,*] , Julian Ng[*,†], Thomas O. Auer[‡], Mathias Pasche[*], Richard Benton[‡], Gregory S. X. E. Jefferis[2,*], Sebastian Cachero[1,2,*]

[*]Neurobiology Division, MRC Laboratory of Molecular Biology, Cambridge, CB2 0QH, UK

[†]Department of Zoology, University of Cambridge, Cambridge, CB2 3EH, UK

[‡]Center for Integrative Genomics, Faculty of Biology and Medicine, University of Lausanne, CH-1015 Lausanne, Switzerland.

[1] These authors contributed equally to this work.

[2] Corresponding authors

Running title: Second generation chemical labeling

Keywords: immunohistochemistry, chemical labeling, chemical tags, neural circuits, protein labeling, fluorescence microscopy

Correspondence:

- Gregory Jefferis, Division of Neurobiology, MRC Laboratory of Molecular Biology, Francis Crick Avenue, Cambridge, CB2 OQH, UK, phone: +44(0)1223 267000, email: jefferis@mrc-lmb.cam.ac.uk.

- Sebastian Cachero, Division of Neurobiology, MRC Laboratory of Molecular Biology, Francis Crick Avenue, Cambridge, CB2 OQH, UK, phone: +44(0)1223 267000, email: scachero@mrc-lmb.cam.ac.uk.

Labeling and visualizing cells and sub-cellular structures within thick tissues, whole organs and even intact animals is key to studying biological processes. This is particularly true for studies of neural circuits where neurons form sub-micron synapses but have arbors that may span millimeters in length. Traditionally labeling is achieved by immunofluorescence; however diffusion of antibody molecules (>100 kDa) is slow and often results in uneven labeling with very poor penetration into the centre of thick specimens; these limitations can be partially addressed by extending staining protocols to over a week (*Drosophila* brain) and months (mice). Recently we developed an alternative approach using genetically encoded chemical tags CLIP, SNAP, Halo and TMP for tissue labeling; this resulted in >100 fold increase in labeling speed in both mice and *Drosophila*, at the expense of a considerable drop in absolute sensitivity when compared to optimized immunofluorescence staining. We now present a second generation of UAS and LexA responsive CLIP, SNAPf and Halo chemical labeling reagents for flies. These multimerized tags with translational enhancers display up to 64 fold increase in sensitivity over first generation reagents. In addition we developed a suite of conditional reporters (4xSNAPf tag and CLIP-SNAP-Halo) that are acti-

vated by the DNA recombinase Bxb1. Our new reporters can be used with weak and strong GAL4 and LexA drivers and enable stochastic, intersectional and multicolor Brainbow labeling. These improvements in sensitivity and experimental versatility, while still retaining the substantial speed advantage that is a signature of chemical labeling, should significantly increase the scope of this technology.

1 Introduction

Visualizing molecules in intact tissues with high sensitivity and specificity is of paramount importance in many fields of biological research. Traditionally cellular and subcellular labeling has depended on immunostaining that combines primary antibodies specific to a molecule of interest, followed by labeled secondary antibodies. Recently we and others have adapted chemical labeling approaches that were initially developed for *in vitro* or single cell studies (Keppler et al., 2003; Gautier et al., 2008; Los et al., 2008) for use in genetically defined cells within intact fly and mouse tissues (Kohl et al., 2014; Yang et al., 2015). These overcame a fundamental limitation of antibodies: low diffusion rate that causes poor penetration of thick tissue samples. The basic principle of chemical labeling is the use of small protein tags (engineered from enzymes) that can covalently and irreversibly bind small molecule substrates. These substrates can be conjugated with a variety of labels such as fluorophores for light microscopy and colloidal gold for electron microscopy (Keppler et al., 2003; Gautier et al., 2008; Vistain et al., 2016). High efficiency binding in combination with small substrate size allows easy tissue penetration and fast quantitative staining (Kohl et al., 2014).

Improvements in speed and penetration achieved by the first generation of chemical labeling reagents are particularly important in neural circuit research where labeling of neurons in deep structures within intact brains is essential for understanding connected networks in the brain but experimentally very challenging. To illustrate this point, optimal immunostaining of a fly brain takes more than a week (Ostrovsky et al., 2013) while a mouse brain can take months even when combined with tissue clearing methods (Chung et al., 2013). In contrast, multicolor chemical labeling of a fly brain can be completed within 1 hour, with less than 10 minutes of staining time. Other important advantages of chemical labeling are that it reduces off-target labeling and

as completely synthetic reagents, in contrast to antibodies, they are not produced using animals. In comparison to the use of genetically encoded fluorescent proteins, reporter lines with chemical labeling transgenes enable rapid testing and switching to new fluorophores with properties required for constantly evolving imaging modalities. While the published *Drosophila* reagents offer unparalleled staining speed (Kohl et al., 2014), they produce considerably weaker signal than traditional immunolabeling of genetically encoded reporters, limiting their use to relatively strong Gal4 driver lines (Brand and Perrimon, 1993). We now introduce a second generation of fly reagents with greatly increased sensitivity. Furthermore, we have increased the versatility of the system by developing reporters for the LexA-based expression system (Lai and Lee, 2006) and reagents for conditional and stochastic labeling based on Bxb1 DNA recombinase (Huang et al., 2011). Finally we show the utility of chemical labeling in targeting challenging tissues such as the fly antennae. We expect these new tools will greatly increase the use of chemical labeling within the research community, especially speeding up projects that require large numbers of stainings.

2 Materials and Methods

2.1 Drosophila stocks

Fly stocks were maintained at 25° on iberian food. The driver lines used in this study are MZ19-Gal4 (Ito et al., 1998), MB247-Gal4 (FlyBaseID: FBst0050742), Fru-Gal4 (gift from Barry Dickson) (Stockinger et al., 2005), BG57-Gal4 (FlyBaseID: FBst0032556), GMR50A02-Gal4 (FlyBaseID: FBti0136386), GMR54F05-Gal4 (FlyBaseID: FBst0039080), GMR59F02-Gal4 (FlyBaseID: FBst0039221), OR22a-Gal4 (gift from Leslie Vossall lab) (Vosshall et al., 2000), IR84a-Gal4 (gift from Richard Benton) (Silbering et al., 2011), Orco-LexA::VP16 (gift from Tzumin Lee) (Lai and

Lee, 2006), GH146-LexA::GAD (gift from Tzumin Lee) (Lai et al., 2008), nSyb-LexA::P65 in attP40 (Pfeiffer et al., 2012), MB247-LexA (Pitman et al., 2011). The reporter lines used in this study are UAS-CD4::CLIPf on 2nd and 3rd, UAS-myr::SNAPf in attP40 and attP2, UAS-myr::Halo2 in attP40 (Kohl et al., 2014), for details of the new reporter lines generated in this study see Table S1. All images are of female brains, apart from the brains in Figure 4d which are male, all flies were dissected 3-4 days after eclosion.

2.2 Drosophila constructs and transgenic flies

Drosophila transformation plasmids from Table 1 were made by Gibson assembly (Gibson et al., 2009) (Figures S4 to S13) or restriction enzyme cloning (Figures S14 to S19). Figures S4 to S19 show the primers and enzymes used to make each plasmid. Transgenic flies were made by BestGene.

Plasmid name	**Genebank accesion no.**	**cloning schematic**
UAS-myr::4xCLIPf	to be added	**Figure S6**
LexAop2-myr::4xCLIPf	to be added	**Figure S8**
UAS-myr::4xSNAPf	to be added	**Figure S7**
LexAop2-myr::4xSNAPf	to be added	**Figure S9**
UAS-myr::>HA-BxbSTOP>myr::4xSNAPf	to be added	**Figure S10**
LexAop2-myr::>HA-BxbSTOP>myr::4xSNAPf	to be added	**Figure S11**
HeatShock-Bxb1-SV40	to be added	**Figure S4**
HeatShock-Bxb1	to be added	**Figure S12**
pJFRC-MUH-stop cassette bxbp	to be added	**Figure S13**
JFRC-MUH-FRT-bxbp	to be added	**Figure S13**
JFRC81-BxbCassette_Clip_Snap_Halo	to be added	**Figure S5**
UAS-Halo7::CAAX	to be added	**Figure S14**
UAS-3xHalo7::CAAX	to be added	**Figure S15**
UAS-7xHalo7::CAAX	to be added	**Figure S16**
UAS-Syt::Halo7	to be added	**Figure S17**
UAS-3xSyt::Halo7	to be added	**Figure S18**
UAS-7xSyt::Halo7	to be added	**Figure S19**
UAS-LA::Halo2	to be added	**Figure S20**

Table 1: **Drosophila transformation plasmids.**

2.3 Labeling Reagents

Substrates were acquired either as stock solutions (e.g., HaloTag-TMR) or in powdered form (SNAPf and CLIPf substrates) and diluted/dissolved in anhydrous dimethyl sulfoxide (DMSO) (Life Technologies) to a concentration of 1 mM. Aliquots (5 µL) were stored at −20° in the presence of desiccant. We observed that using old DMSO or storing dissolved substrates in moist and/or warm conditions can lead to hydrolysis, reducing labeling efficiency. For a list of all substrates used in this study see Table 2.

Substrate (abbreviation)	**Fluorophore**	**Ex**	**Em**	**Binds to**	**Cell permeable**	**Supplier**	**Cat. #**
SNAP-Cell 647-SiR (SNAP-SiR)	SiR	645	661	SNAPm/f	Yes	NEB	S9102S
SNAP-Surface 549 (SNAP-549)	Dyomics DY-549P1	560	575	SNAPm/f	No	NEB	S9112S
CLIP-Surface 488 (CLIP-488)	ATTO-TEC 488	506	526	CLIPm/f	No	NEB	S9232S
CLIP-Surface 547 (CLIP-547)	Dyomics DY-547	554	568	CLIPm/f	No	NEB	S9233S
HaloTag TMR Ligand (Halo-TMR)	TMR	555	585	Halo2/7	Yes	Promega	G8252
HaloTag SiR Ligand (Halo-SiR)	SiR	645	661	Halo2/7	Yes	K. Johnsson	n/a

Table 2: **Chemical Tagging Substrates used in this study.** Commercially available, fluorophore-coupled substrates for SNAP-, CLIP- and Halo- are listed.

2.4 Protocol for labeling Drosophila Brains

Single and double channel labeling of Drosophila brains was carried out as previously described (Kohl et al., 2014). For labeling of UAS-LA::Halo2 fillet preparation of wandering third instar larvae were made followed by the same protocol used for labeling whole brains. For detailed information on staining Chemical Brainbow brains and antennal segments see Supplemental Information. We find that CLIPf substates

weakly bind SNAPf tag, therefore if labeling both SNAPf and CLIPf in the same specimen we recommend doing sequential SNAPf substrate incubation (minimum 5 min) then addition of CLIPf substrate (minimum 5 min), to avoid cross reactivity.

2.5 Image Acquisition and Deconvolution

Confocal stacks of fly brains were imaged at 768 × 768 pixels every 1 µm (voxel size of 0.46 × 0.46 × 1 µm; 0.6 zoom factor) using an EC Plan-Neofluar 40×/1.30 Oil DIC M27 objective and 16-bit color depth. Higher magnification images of cell bodies were acquired at 2048 × 2048 pixels every 0.45 µm (voxel size 0.1 × 0.1 × 0.45 µm; 1.0 zoom factor) using a Plan-Apochromat 63x/1.40 Oil DIC M27 objective and 16-bit color depths. Antennae were imaged at 1024 × 1024 pixels every 1 µm (voxel size 0.20 × 0.20 × 1 µm; 1.0 zoom factor) using an EC Plan-Neofluar 40×/1.30 Oil DIC M27 objective and 8-bit color depths. The image of the entire larval musculature (Figure 5b) was acquired as a tile scan with total dimensions 1536 x 2304 pixels every 1.0 µm (voxel size 1.84 × 1.84 × 1.0 µm; 0.6 zoom factor) with EC Plan-Neofluar 10x/0.30 M27 objective and 16-bit color depths. The high magnification larval muscle inset was acquired at 2156 × 2156 pixels every 0.45 µm (voxel size 0.1 × 0.1 × 0.45 µm; 1.0 zoom factor) using a Plan-Apochromat 63x/1.40 Oil DIC M27 objective and 16-bit color depth. All images acquired on a Zeiss LSM710 confocal microscope.

The confocal stack of the fly brain in Figure 1d was acquired using a Leica SP8 confocal microscope, following the Nyquist criterion, at 4224 x 4224 pixels every 0.313 µm (voxel size 0.076 × 0.076 × 0.313 µm; 0.9 zoom factor) using a HC PL APO CS2 40x/1.30 oil objective. Image deconvolution was carried out on each channel individually using the Huygens Professional (Scientific Volume Imaging) software with a backprojected pinhole of half the emission wavelength in nm, a theoretical Point Spread Function, automatic back ground estimation, 5 Iterations, a Signal to noise ration of 20, a Quality threshold of 0.05, optimized Iteration mode and an automatic

brick layout. The separate deconvolved channels were then combined as an RGB tiff using Fiji (Schindelin et al., 2012).

2.6 Fluorescence quantification

For the comparison between old and new reporters we acquired confocal stacks using two different 561 nm laser power settings (low 2% and high 10%) with gain (600) and pinhole (60.1 µm, 1.42 AU) remaining constant. Images acquired at the low setting were optimal for non-saturated images of the new reporters and images acquired at the high setting were optimal for the old reporters so that we had a stack that could be segmented for quantification and then the data from the low stacks were quantified (see below). Confocal .lsm files were then converted to .nrrd files using Fiji. Using Amira 6.0.1 (FEI, Thermo Fisher Scientific) a .nrrd stack, for each brain to be quantified, was opened (high versions for the old reported and low versions for the new reporters) and a median filter of 3 iterations was applied. Using the Segmentation Editor in Amira 6.0.1, two materials were assigned to the median filtered stack for each brain: 1) for quantifying signal a three dimensional ROIs surrounding the axonal terminals of Mz19-Gal4 PNs in the lateral horn, 2) for background correction a three dimensional region ventral to the axonal terminals of Mz19-Gal4 PNs in the lateral horn.The intensity and background correction calculations were performed in R (Team, 2016) and detailed in R Markdown supplemental file. Briefly, for comparison of the old and new CLIPf reporters we used the average intensity in the LH of the old reporters as baseline and then divided the quantified intensity of the new reporter by the average for the old reporters to give a fold change (e.g. for the comparison of new 4xCLIPf in attP40 with the old version of the CLIPf reporters: the intensity value of 4xCLIPf in attP40 was divided by the average of the intensities calculated for both insertions of the old version CLIPf reporters, see the R Markdown supplemental file for details of the calculations). For new vs old comparisons of the Halo reporters we

calculated percentage change as this was a more meaningful comparison (see the R Markdown supplemental file for details of the calculations).

3 Data Availability

All data necessary for confirming the conclusions presented in the article are represented fully within the article. All fly strains and plasmids are available upon request. Sequence data for all plasmids will be made available at GenBank and the accession numbers listed in Table 1. Code used to quantify fluorescence intensities is provided in File S1.

4 Results

4.1 New CLIPf and SNAPf reporters with increased sensitivity

The first generation of chemical labeling reporters achieved rapid staining times, shortening protocols from over 100 hours to less than 1 hour for whole mount *Drosophila* brains (Kohl et al., 2014). Despite this dramatic improvement in staining speed, signal strength is lower than antibody staining of reporter proteins. This is likely due to the non-amplifiying nature of chemical labeling: one molecule of tag covalently binds one substrate molecule fused to one molecule of fluorophore. This linearity can be beneficial when quantifying signal intensity. In contrast, with immunofluorescence one target can be bound by more than one primary antibody which is then recognized by several secondary antibody molecules each conjugated to multiple fluorophores leading to substantial signal amplification. This lower sensitivity is evident when comparing the signal from several Gal4 lines (Rubin collection, Janelia

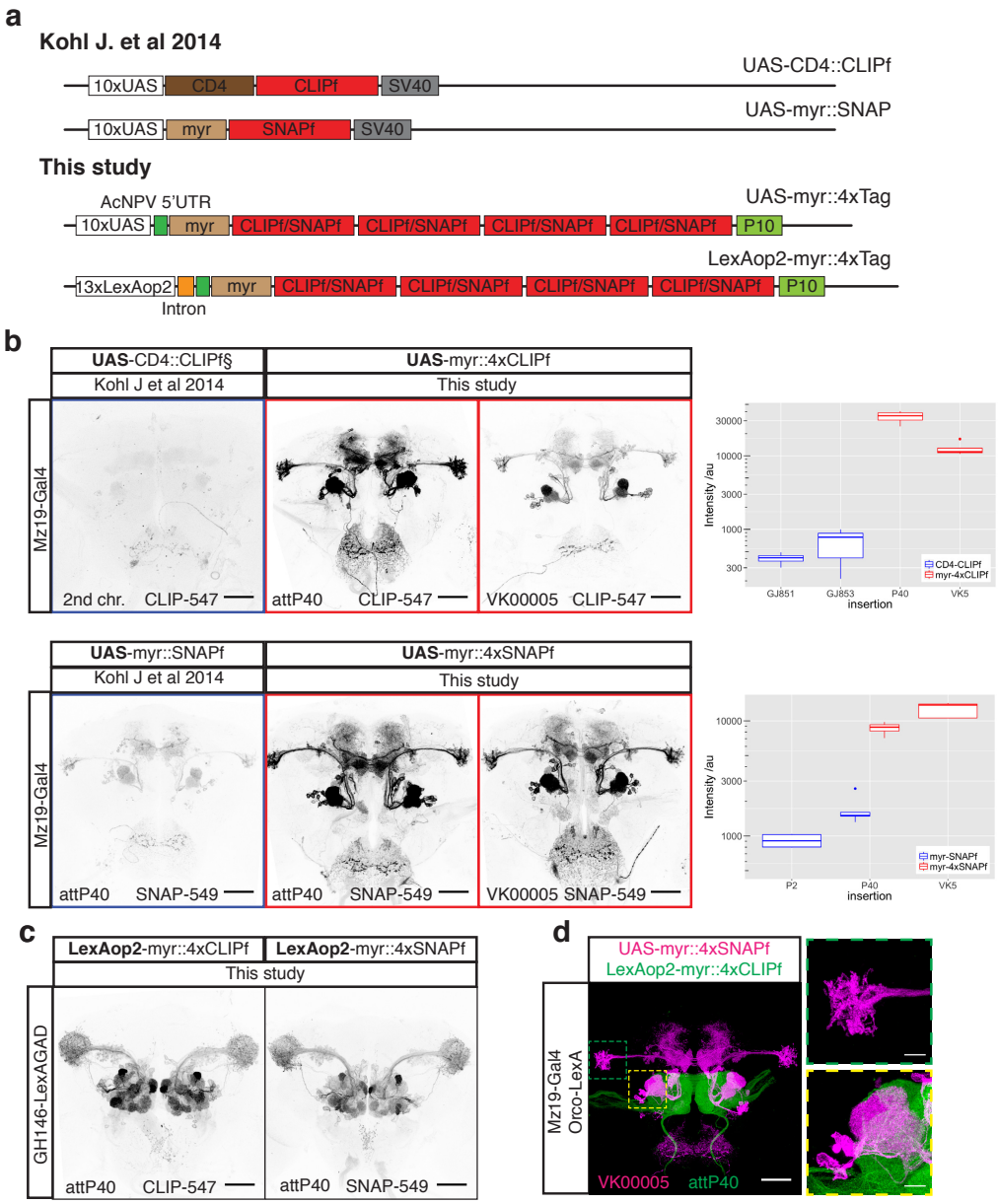

Figure 1: **New CLIPf and SNAPf reporters have increased sensitivity.** **(a)** Schematic of previous CLIPf/SNAPf reporters from (Kohl et al., 2014) and the new reporters from this study. **(b)** Labeling of Mz19-Gal4 neurons using the old and new reporters. Each panel contains information on the dye used and insertion sites. Box plots show the quantification of fluorescence intensity of the axonal terminals of projection neurons in the lateral horn (arbitrary units). Boxplot n numbers were; GJ853 CD4::CLIPf on 2nd n=3, GJ851 CD4::CLIPf on 3rd n=4, P40 myr::4xCLIPf n=4, VK00005 myr::4xCLIPf n=4, P40 myr::4xSNAPf n=4, VK00005 myr::4xSNAPf n=5, P2 myr::SNAPf n=4 and P40 myr::SNAPf n=5 **(c)** New LexAop2-myr::4xCLIPf/4xSNAPf reporters labeling olfactory projection neuron using the weak GH146-LexA::GAD driver. **(d)** Orthogonal labeling of olfactory sensory neurons (green) and projection neurons (magenta) using new tags. Shown is the max intensity projection of a confocal stack after deconvolution. Images in panels b and c were acquired using the same microscope settings. Scale bars are 50 µm in whole brain images and 10 µm in higher magnification images of the boxed areas in panel d.

Research Campus) driving GFP or first generation CLIPf and SNAPf reporters (Figures S1a and S2a). To bridge this gap and extend the use of chemical labeling to most Gal4 driver lines, weak and strong, we designed a new generation of reporters with greatly increased sensitivity. These reporters differ from the original ones in two ways: first, they have a short 5' UTR (AcNPV) and the 3' UTR from the *A. californica nucleopolyhedrovirus* P10 gene; these modifications have been shown to increase translational efficiency by more than 20 times (Pfeiffer et al., 2012) and second, they are tetramerized to increase reporter signal up to four fold (Shearin et al., 2014) (Figure 1a). We generated transgenic fly lines by inserting these new 4xCLIPf and 4xSNAPf reporters into the well-characterized attP40 and VK00005 phiC31 landing sites on the 2nd and 3rd chromosomes, respectively (Table S1).

We tested these new transgenes and compared them to the first generation reporters using the sparse line Mz19-Gal4, a driver of medium strength that expresses in about 12 olfactory projection neurons innervating three adjacent olfactory glomeruli and a group of neurons with processes near the mushroom bodies. When driven by Mz19-Gal4 all reporters produced the expected labeling pattern. In comparison, the first generation tags were barely visible when imaged under conditions that produced strong signal with the new reporters (Figure 1b). To quantify the increase in signal strength we measured intensity in the axonal terminals of projection neurons in the lateral horn (green dotted area in Figure 1d, see methods). Using the average between UAS-CD4::CLIPf on the 2nd and 3rd chromosomes as baseline, the new UAS-myr::4xCLIPf reporters are 64 (attP40) and 24 (VK00005) times brighter. In the case of SNAP, the new UAS-myr::4xSNAPf reporters are 7 (attP40) and 10 (VK00005) times brighter than the average between the first generation UAS-myr::SNAPf in attP2 and attP40. While CLIPf and SNAPf substrates use different fluorophores and have different labeling sensitivities, complicating precise quantitative comparisons, the new CLIPf and SNAPf reporters produced qualitatively similar fluorescence in-

tensities. To extend these results to other driver lines we used a number of Gal4 P element and enhancer fusion insertions of varying strengths to drive the new reporters (weakest to strongest: GMR-50A02-Gal4, GMR-59F02-Gal4 and GMR-54F05-Gal4). Qualitatively these stainings recapitulated the Mz19-Gal4 results with the new reporters showing large increases in brightness (Figure S1 and S2). These results indicate the new reporters are suitable for labeling most if not all Gal4 driver lines that show expression after immunostaining.

4.2 LexA responsive reporters

Dissecting the function of neuronal components in a circuit often requires labeling more than one cell population with different reporters that respond to orthogonal drivers such as Gal4 and LexA. To increase the flexibility of the chemical labeling platform we made LexA responsive tetramerized CLIPf and SNAPf reporters and inserted them in attP40 and VK00005 (Table S1). We tested these reporters using the weak driver line GH146-LexA::GAD. We found that LexAop2-myr::4xCLIPf and LexAop2-myr::4xSNAPf reporters inserted in both chromosomal locations produced strong labeling (Figure 1c and Figure S2c). Since new LexA drivers are now routinely made with the strong p65 transactivation domain rather than the weaker GAD domain, this result suggests our new reporters will be useful for most LexA driver lines. Finally, we show how these new reagents can be used for visualizing different cell populations by labeling olfactory sensory neurons (Orco-LexA::VP16) and a subset of their post-synaptic projection neurons (Mz19-Gal4) in the same brain (Figure 1d). While we imaged this brain using a confocal microscope (following the Nyquist criterion and subsequent deconvolution, see methods), super-resolution microscopy techniques, such as STED, could also be used, when available for thick tissue specimens, to increase resolution.

4.3 New Halo tag reporters with improved membrane localization and signal strength

Our first generation Halo tag reporters already incorporated the 5' and 3' translational enhancers L21 and P10 (Figure 2a) and were inserted into PhiC31 landing sites that support strong expression (attP40 and attP2). While this tag produced the brightest signal among the first generation of chemical reporters we noticed an unexpected accumulation of the tag in the cell nucleus and reduced signal in axons (Figure 2b) suggesting suboptimal cellular localization. Intriguingly, 4xCLIPf and 4xSNAPf tags use the same myristoylation signal as Halo (first 90 amino acids from the *Drosophila* Src protein) but are excluded from the nucleus, displaying the expected membrane localization. In order to improve cellular localization we replaced the N-terminal myristolation with a C-terminal CAAX membrane targeting signal (Choy et al., 1999). In addition we made several reporters with either one, three and seven tandem fusion-tags of Halo with the aim of increasing labeling efficiency (Figure 2a) . The new constructs use Halo version 7 (Halo7) which is reported to show increased expression, stability and substrate binding kinetics over version 2 (Halo2) (Encell et al., 2012). We made transgenic flies with insertions in attP40, VK00005 and VK00027 (Table S1).

We compared cellular localization and signal intensities from the first and new generation of Halo tags in the same way as for CLIPf and SNAP. Nuclear signal is greatly reduced in the new CAAX reporters when compared to the myristoylated ones (See higher magnification images from the first two panels of Figure 2b). In addition, we measured modest increases in signal strength with the new monomeric and trimeric reporters (53% and 78% brighter, respectively, Figure 2b, box plot). Surprisingly the heptamer is 28% less bright than the old reporter, possibly due to increased instability or impaired trafficking (Figure 2b, box plot).

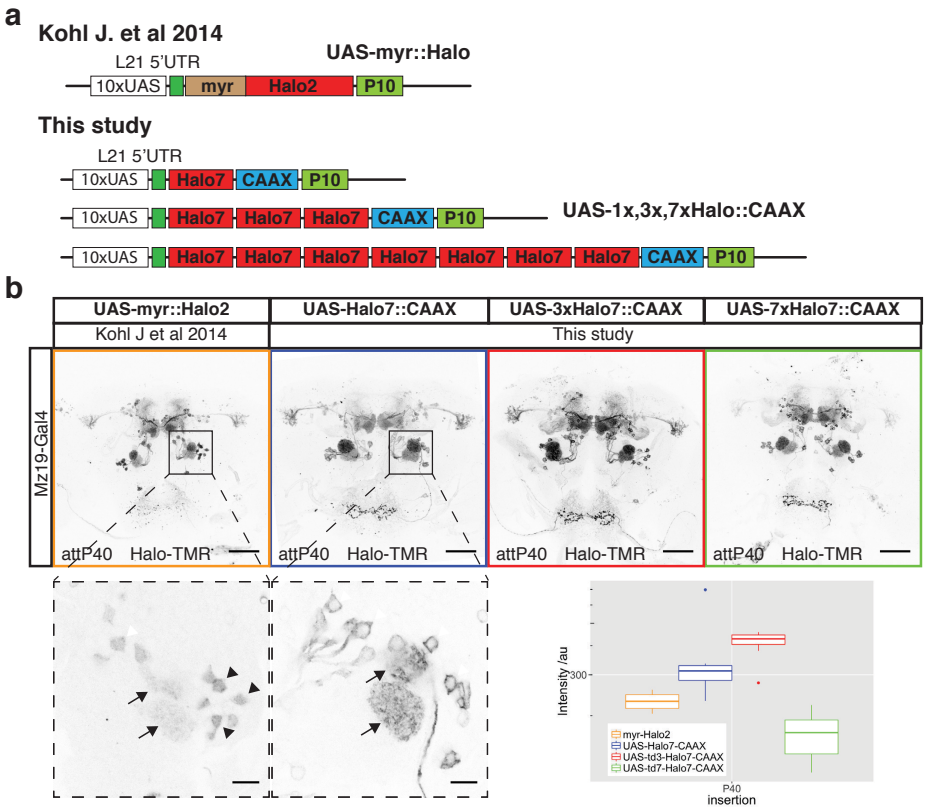

Figure 2: **New Halo reporters with improved sensitivity and localization. (a)** Schematic of CLIP/SNAPf reporters from (Kohl et al., 2014) and the new reporters from this study. **(b)** Labeling of Mz19-Gal4 positive neurons using the old myr::Halo2 and new Halo7::CAAX reporters. All images were aquired using the same microscope settings. Lower panels are high magnification single slice images showing differences in reporter localization in the cell bodies (arrowheads) of olfactory projection neurons. Arrows indicate signal in glomeruli. The box plot shows the quantification of fluorescence intensity of the axonal terminals of PNs in the lateral horn (arbitrary units). Boxplot n numbers were; myr::Halo2 n=7, UAS-Halo7::CAAX-P40 n=7, UAS-3xHalo7::CAAX n=8 and UAS-7xHalo7::CAAX n=8. Scale bars in full brain images are 50 μm and higher magnification images of cell bodies 10 μm.

4.4 Chemical tags in peripheral sensory organs.

We wanted to explore the performance of chemical labeling in tissues other than the brain, where differences in extracellular matrix or other cellular barriers may have a negative impact on labeling. To accomplish this we stained sensory neurons in whole-mount third antennal segments. This tissue is typically regarded as hard to stain in part because it is surrounded by cuticle, in contrast to brains which are dissected out of the head capsule before staining. While immunolabeling can work, as for brains, the optimized protocol spans up to a week (Saina and Benton, 2013). Using GAL4 driver lines that label sensory neurons (Ionotropic receptor 84a (IR84a) and Odorant receptor 22a (Or22a)), we expressed the new 4xSNAPf and 3xHalo7 reporter lines in the antennae (Figure 3 and S3). While reporters produced signal in the expected cells in all cases, shorter labeling incubations produce lower background, especially in the cuticle (Figure 3b, arrowheads). The SNAPf label also resulted in more uniform labeling of the axons and soma when compared to a mCD8::GFP reporter (Figure 3a, arrowheads vs arrows). In contrast to immunostaining, chemical labeling reagents penetrate rapidly as demonstrated by the signal being as strong after 10 minutes as it is after 3 h (Figure 3b). In addition chemical labeling in the antennae, as in the brain (Kohl et al., 2014), can be combined with immunolabeling, in this case of the Or22a receptor (Figure S3).

4.5 Conditional reporters

Brains are densely packed with neurons of great diversity both in morphology and function. A fundamental step in studying complex neural circuits is to break them down into smaller components by visualizing the morphology of single or small clusters of neurons. To achieve this, neuroanatomical studies take advantage of large promoter-Gal4 and LexA collections to find sparse drivers to express reporters in small

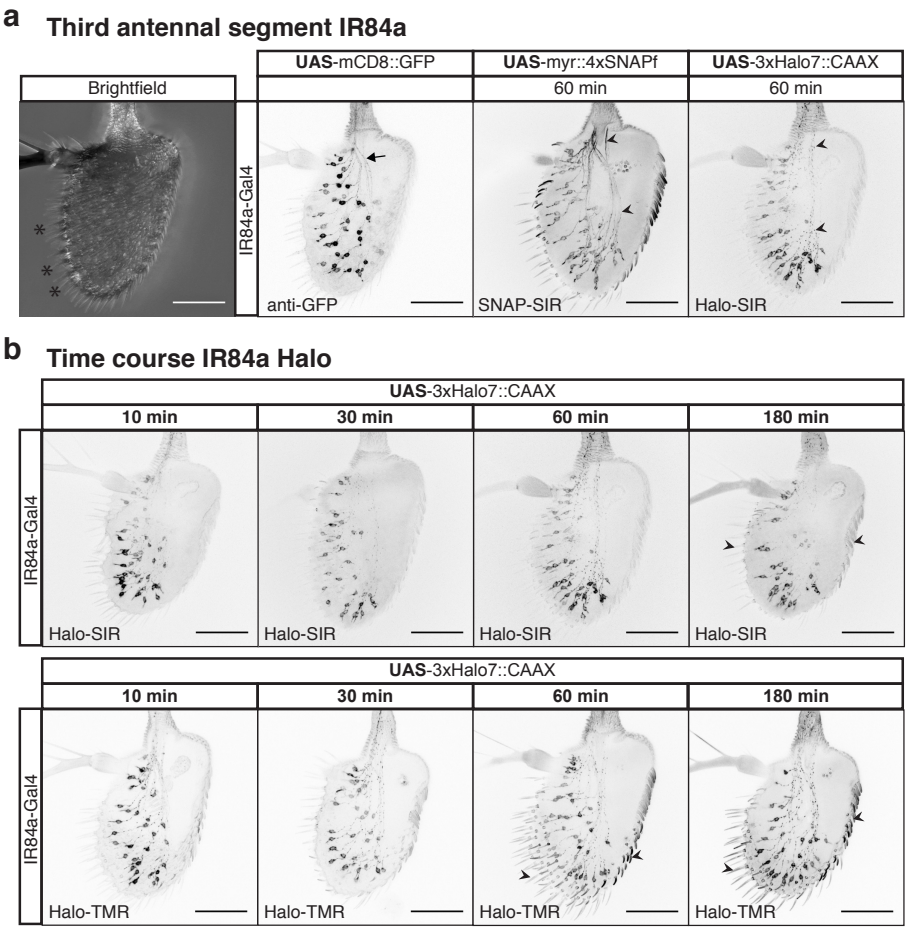

Figure 3: **Chemical tags in peripheral sensory organs. (a)** Left-most image, bright field image of the antennae, sensilla are marked with asterisks. Chemical labeling of Ionotropic Receptor 84a (IR84a) expressing sensory neurons. Comparison between GFP immunostaining and SNAP-SiR chemical labeling; arrow and arrowheads highlight stronger labeling of axons by chemical labeling relative to the soma. **(b)** Incubation time series for far red Halo-SiR (top row) and red Halo-TMR (bottom row) dyes. All panels shows partial projections of confocal stacks that exclude the cuticle. Scale bars are 50 μm.

numbers of neurons. While this approach greatly limits the number of labeled cells, they often have overlapping processes which cannot be resolved by light microscopy. In these cases further labeling refinements, using a number of genetic strategies, are often required (Jefferis and Livet, 2012). We extended the applicability of chemical labeling to these situations by developing reagents to: a) limit the number of labeled cells or b) increase the combinatorial number of fluorophores available for each labelled neuron.

To limit the number of labeled cells we designed an inactive reporter with a transcriptional stop cassette upstream of the coding region for 4xSNAP. This reporter can be activated upon removal of the stop cassette by the DNA recombinase Bxb1 (Figure 4a). We chose Bxb1 from mycobacteriophage (Huang et al., 2011) as it is orthogonal to recombinases commonly used in *Drosophila.* Another advantage is its irreversibility as it recombines attP and attB sites to generate new attL and attR sites which are no longer substrates. We generated lines that express Bxb1 in three different ways: a) stochastically, using a heat shock inducible promoter (hs-Bxb1, Figures S4 and S12), b) by driving its expression with Gal4 (UAS-Bxb1, Figure 4b) and c) by using a combination of Gal4 and Flp DNA recombinase (UAS>FlpSTOP>Bxb1, Table S1).

As a proof of principle we used the conditional reporters in three experiments to intersect the expression of Gal4 and LexA drivers. The schematic in Figure 4b shows the logic of the experiment: MB247-Gal4 or Mz19-Gal4 drives expression of UAS-Bxb1 to activate the conditional reporter LexAop2-myr::>BxbSTOP>4xSNAP; the activated reporter is then driven by MB247-LexA::VP16 or the pan-neuronal nSyb-LexA::p65. In the first experiment, MB247-Gal4 $\cap$ nSyb-LexA::P65, the result is very similar to that of a regular reporter with the exception of the lack of strong glial staining, normally present in MB247-Gal4, due to the reporter being driven by the neuronal specific nSyb-LexA::p65 (compare Figure 4c.i and c.ii). On the other hand, the second experiment shows Mz19-Gal4 $\cap$ nSyb-LexA::P65 is considerably broader

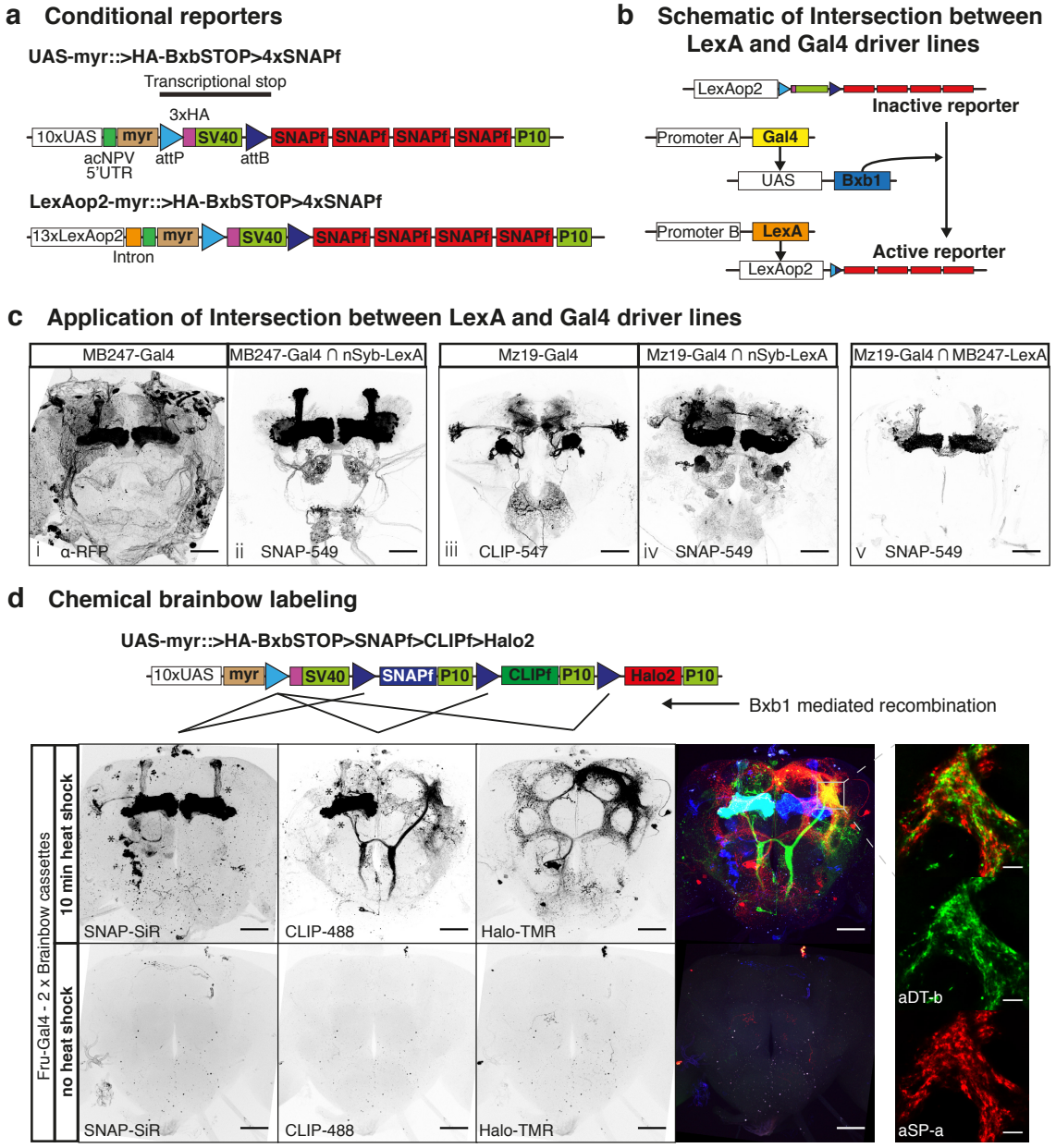

Figure 4: **Sparsening expression using conditional chemical reporters.** **(a)** Schematic of new conditional reporters. The HA tag present in the stop cassette can reveal the expression of the inactive reporter (not shown). **(b)** Schematic showing the genetic approach to intersect LexA and Gal4 in c. **(c)** Panels i and iii show confocal projections of Gal4 lines driving regular reporters. Panels ii and iv show confocal projections of Gal4 lines intersected with the panneuronal nSyb-LexA::P65 using the scheme from b. Panel v shows a confocal projection of the intersections between the sparse lines Mz19-Gal4 and MB247-LexA::VP16. **(d)** Heatshock activation of Brainbow cassettes during early development label neuroblast clones of *fruitless* positive neurons. Bottom panels show the Brainbow cassettes are silent when no heatshock is applied. Asterix indicate the cell bodies form neuroblast clones. Panels on the right: high magnification single confocal slice showing the close apposition between processes from the two sexually dimorphic clones aSP-a and aDT-b. Scale bars for full brain images are 50 μm and scale bars for higher magnifications are 10 μm.

than that of the regular reporter including labeling in the mushroom bodies (compare Figure 4c.iii and c.iv). Mz19-Gal4 ⋂ nSyb-LexA::P65 reflects two interesting properties of this approach: first, it captures and immortalizes developmental expression and second, weakly expressing cells, previously undetectable with a regular reporter, could drive Bxb1 mediated recombination allowing strong reporter expression driven by nSyb-LexA::P65. In the third experiment we used Mz19-Gal4 to activate the reporter and MB247-LexA::VP16 to drive it; as one would predict from the previous two experiments this intersection labels a modest number of mushroom body Kenyon cells (Figure 4c.v).

The second strategy for resolving overlapping processes is multiplexing the label. The approach we took is based on the Brainbow technique (Livet et al., 2007; Hadjieconomou et al., 2011; Hampel et al., 2011) using the tags CLIPf, SNAPf and Halo2 (Figure 4d). Our reporter incorporates translational enhancers without multimerization. We used Bxb1 to activate the cassette as for our single tag conditional reporters. Because Bxb1 recombination is irreversible the cassette requires fewer recombination sites than previous Brainbow reporters. Upon expression of the recombinase, the single attP site recombines with one of the three attB sites removing the intervening DNA and irreversibly selecting one of the three tags for expression (see schematic in Figure 4d) . We made fly lines with the Brainbow cassette inserted into attP2 and VK00005 (Table S1).

We tested the new cassettes by labeling subsets of neurons that express the male specific form of the Fruitless protein (FruM). By activating the Brainbow cassette immediately after larval hatching we aimed to create groups of labeled cells of the same developmental origin (neuroblast clones, see methods). Our pilot experiment showed that both transgenes are efficiently activated producing the expected *fruitless* positive neuroblast clones (Compare Figure 4d with Cachero et al. (2010)). We found that the three chemical tags were activated in a similar number of neuroblast clones

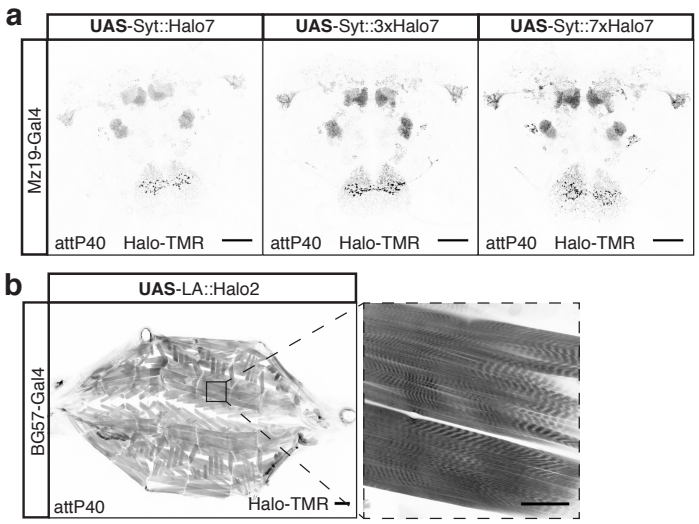

Figure 5: **New sub-cellular Halo reporters. (a)** Labeling the synaptic terminals of Mz19-Gal4 positive neurons using Halo7 reporters fused to Synaptotagmin. **(b)** Labeling of muscle actin in the larva using a fusion between Halo2 and LifeAct peptide. Scale bars in full brain images and higher magnification of muscle fibre are 50 μm and full larva 200 μm.

(marked with asterisks in Figure 4d: 3 clones for SNAPf, 3 for CLIPf 3 and 2 for Halo2). The presence of both Brainbow cassettes can can be seen in the mushroom body clone on the fly's right side where both CLIPf and SNAPf tags were activated, labeling the resulting clone in cyan. Resolving several clones in a single brain has the advantage of requiring fewer samples to describe the anatomy of a neuronal population. Furthermore it enables researchers to examine the overlap between clones within the same brain rather than using image registration and post hoc comparisons of clones from multiple brains. For instance, it makes possible to examine the close apposition of processes from aSP-a and aDT-b clones in the male enlarged region of the brain (Figure 4d, high magnification insets).

4.6 Sub-cellular reporters

Encouraged by the good results obtained while labeling membranes, we wanted to make reporters for other cellular compartments, both in the nervous system and

elsewhere.

Synapses are the key sites of information transfer in neuronal circuits. In order to label them we made UAS reporters where one, three or seven copies of the Halo7 tag are fused to the pre-synaptic protein Synaptotagmin (Syt, Table S1). When driven by Mz19-Gal4 all three Syt::Halo7 synaptic markers produced strong labeling in areas known to have presynapses with minimal presence in regions devoid of them (compare Figure 2b and 5a). The gradation in signal strength going from monomer to heptamer makes these reporters useful for labeling synapses using drivers ranging from weak to strong.

Next, we made a reporter for fast and sensitive labeling of actin filaments by fusing a peptide, LifeAct (LA) that binds actin filaments to Halo2 (Table S1) (Riedl et al., 2008). As a proof of principle we expressed the reporter using the pan-muscular driver BG57-Gal4. These larvae are viable despite widespread expression of LA::Halo2, indicating the reporter is not overtly toxic. The staining of body wall muscles in third instar larvae revealed the expected expression pattern with stripes of muscle actin bundles clearly visible (Figure 5b).

5 Discussion

In this study we introduce a second generation of chemical tags that achieve substantial improvements in sensitivity and versatility over the first generation. Most applications where tag immunostaining is used can benefit from super fast and highly sensitive chemical labeling and the new reagents are ideally suited for medium to high throughput applications such as anatomical screens of driver lines or assessment of RNAi screen phenotypes.

The introduction of LexAop2 and conditional reporters opens the possibility to a larger set of experiments than was possible with first generation reagents. For instance

combining UAS and LexAop2 reporters will allow super-resolution microscopy to resolve potential contacts between different neuronal populations. The Brainbow cassette can be used in large anatomical screens enabling rapid characterization of complex driver lines by labeling multiple clones in the same brain (Livet et al., 2007; Hadjieconomou et al., 2011; Hampel et al., 2011). Besides the increase in speed, this allows imaging different neuronal populations in the same brain offering a powerful insight into their potential connectivity. Our conditional reporters can be used to capture developmental expression; these could be exploited for a systematic study of neuronal fate during metamorphosis. While we validated our reagents in the antennae it is likely that chemical labeling will work in most other tissues. Beyond the field of neuroscience the chemical actin reporter will be a useful alternative to the widely used but highly toxic phalloidin staining, particularly in those applications where genetically targeting to specific muscles could be an advantage. A second advantage is the irreversible nature of the chemical staining, while phalloidin stainings fade with time. Lastly, it could be used for *in-vivo* imaging when combined with cell permeable substrates.

The improvements in signal strength achieved by the new reagents derive from their higher expression levels. For experiments where an even stronger signal is needed more than one transgene could be used. In the case of the Brainbow cassettes we are currently multimerizing the tags to obtain higher signal to noise ratio. Another possibility would be developing brighter ligands, for instance by conjugating multiple fluorophores per ligand molecule . The collection of reagents presented here is by no means exhaustive, further additions to this toolkit could include generation of reporters to harness the QUAS system (Potter et al., 2010) and expansion of the multimerized chemical tags to target sub-cellular compartments and organelles; for example axons, dendrites, microtubules and mitochondria.

While the new chemical tags were successful in producing strong labeling of all Gal4

and LexA lines tested, a new comparison between chemical labeling and smFP immunolabeling (Viswanathan et al., 2015) found that the latter still yields better signal to noise ratio than a single copy multimerized chemical tag (Meissner G., personal communication). This is unsurprising as the smFPs are one of the most optimized tags available for immunostaining with 10-15 copies of their epitope tags which are then subjected to a highly optimized, but long (>10 days), staining protocol. Therefore, in our view the significant increase in speed and reproducibility derived from the simple chemical labeling protocol, coupled with strong signal make it an attractive option for most applications.

In conclusion, the new reagents generated in this study significantly extend the experimental reach of chemical labeling to most forms of genetic labeling scenarios in *Drosophila*. This should significantly increase its use by the research community. We hope that this will also encourage non-*Drosophila* researchers to expand and optimize the use of chemical labeling in other genetic model organisms.

6 Acknowledgements

We thank members of the G.S.X.E.J. lab for comments on the manuscript. This work was supported by the Medical Research Council [MRC file reference U105188491 and U105178788], European Research Council Starting Investigator (211089) and Consolidator Grants (649111) to G.S.X.E.J and a Royal Society Dorothy Hodgkin Fellowship to S.C.. T.O.A. is supported by a Human Frontier Science Program Long Term Fellowship. Research in R.B.'s laboratory is supported by the University of Lausanne and an ERC Consolidator Grant (615094). Stocks obtained from the Bloomington Drosophila Stock Center (NIH P40OD018537) were used in this study.

7 Bibliography

References

Brand, A. H., Perrimon, N., Jun 1993. Targeted gene expression as a means of altering cell fates and generating dominant phenotypes. Development 118 (2), 401–15.

Cachero, S., Ostrovsky, A. D., Yu, J. Y., Dickson, B. J., Jefferis, G. S. X. E., Sep 2010. Sexual dimorphism in the fly brain. Curr Biol 20 (18), 1589–1601.

Choy, E., Chiu, V. K., Silletti, J., Feoktistov, M., Morimoto, T., Michaelson, D., Ivanov, I. E., Philips, M. R., Jul 1999. Endomembrane trafficking of ras: the caax motif targets proteins to the er and golgi. Cell 98 (1), 69–80.

Chung, K., Wallace, J., Kim, S.-Y., Kalyanasundaram, S., Andalman, A. S., Davidson, T. J., Mirzabekov, J. J., Zalocusky, K. A., Mattis, J., Denisin, A. K., Pak, S., Bernstein, H., Ramakrishnan, C., Grosenick, L., Gradinaru, V., Deisseroth, K., May 2013. Structural and molecular interrogation of intact biological systems. Nature 497 (7449), 332–7.

Encell, L. P., Friedman Ohana, R., Zimmerman, K., Otto, P., Vidugiris, G., Wood, M. G., Los, G. V., McDougall, M. G., Zimprich, C., Karassina, N., Learish, R. D., Hurst, R., Hartnett, J., Wheeler, S., Stecha, P., English, J., Zhao, K., Mendez, J., Benink, H. A., Murphy, N., Daniels, D. L., Slater, M. R., Urh, M., Darzins, A., Klaubert, D. H., Bulleit, R. F., Wood, K. V., 2012. Development of a dehalogenase-based protein fusion tag capable of rapid, selective and covalent attachment to customizable ligands. Curr Chem Genomics 6, 55–71.

Gautier, A., Juillerat, A., Heinis, C., Corrêa, Jr, I. R., Kindermann, M., Beaufils, F., Johnsson, K., Feb 2008. An engineered protein tag for multiprotein labeling in living cells. Chem Biol 15 (2), 128–36.

464 Gibson, D. G., Young, L., Chuang, R.-Y., Venter, J. C., Hutchison, 3rd, C. A., Smith,
465 H. O., May 2009. Enzymatic assembly of dna molecules up to several hundred
466 kilobases. Nat Methods 6 (5), 343–5.

467 Hadjieconomou, D., Rotkopf, S., Alexandre, C., Bell, D. M., Dickson, B. J., Salecker,
468 I., Mar 2011. Flybow: genetic multicolor cell labeling for neural circuit analysis in
469 drosophila melanogaster. Nat Methods 8 (3), 260–6.

470 Hampel, S., Chung, P., McKellar, C. E., Hall, D., Looger, L. L., Simpson, J. H., Mar
471 2011. Drosophila brainbow: a recombinase-based fluorescence labeling technique to
472 subdivide neural expression patterns. Nat Methods 8 (3), 253–9.

473 Huang, J., Ghosh, P., Hatfull, G. F., Hong, Y., Sep 2011. Successive and targeted
474 dna integrations in the drosophila genome by bxb1 and phic31 integrases. Genetics
475 189 (1), 391–5.

476 Ito, K., Suzuki, K., Estes, P., Ramaswami, M., Yamamoto, D., Strausfeld, N. J., 1998.
477 The organization of extrinsic neurons and their implications in the functional roles
478 of the mushroom bodies in drosophila melanogaster meigen. Learn Mem 5 (1-2),
479 52–77.

480 Jefferis, G. S. X. E., Livet, J., Feb 2012. Sparse and combinatorial neuron labelling.
481 Curr Opin Neurobiol 22 (1), 101–10.

482 Jenett, A., Rubin, G. M., Ngo, T.-T. B., Shepherd, D., Murphy, C., Dionne, H.,
483 Pfeiffer, B. D., Cavallaro, A., Hall, D., Jeter, J., Iyer, N., Fetter, D., Hausenfluck,
484 J. H., Peng, H., Trautman, E. T., Svirskas, R. R., Myers, E. W., Iwinski, Z. R.,
485 Aso, Y., DePasquale, G. M., Enos, A., Hulamm, P., Lam, S. C. B., Li, H.-H.,
486 Laverty, T. R., Long, F., Qu, L., Murphy, S. D., Rokicki, K., Safford, T., Shaw, K.,
487 Simpson, J. H., Sowell, A., Tae, S., Yu, Y., Zugates, C. T., Oct 2012. A gal4-driver
488 line resource for drosophila neurobiology. Cell Rep 2 (4), 991–1001.

489 Keppler, A., Gendreizig, S., Gronemeyer, T., Pick, H., Vogel, H., Johnsson, K., Jan
490 2003. A general method for the covalent labeling of fusion proteins with small
491 molecules in vivo. Nat Biotechnol 21 (1), 86–9.

492 Kohl, J., Ng, J., Cachero, S., Ciabatti, E., Dolan, M.-J., Sutcliffe, B., Tozer, A.,
493 Ruehle, S., Krueger, D., Frechter, S., Branco, T., Tripodi, M., Jefferis, G. S. X. E.,
494 Sep 2014. Ultrafast tissue staining with chemical tags. Proc Natl Acad Sci U S A
495 111 (36), E3805–14.

496 Lai, S.-L., Awasaki, T., Ito, K., Lee, T., Sep 2008. Clonal analysis of drosophila anten-
497 nal lobe neurons: diverse neuronal architectures in the lateral neuroblast lineage.
498 Development 135 (17), 2883–93.

499 Lai, S.-L., Lee, T., May 2006. Genetic mosaic with dual binary transcriptional systems
500 in drosophila. Nat Neurosci 9 (5), 703–9.

501 Livet, J., Weissman, T. A., Kang, H., Draft, R. W., Lu, J., Bennis, R. A., Sanes, J. R.,
502 Lichtman, J. W., Nov 2007. Transgenic strategies for combinatorial expression of
503 fluorescent proteins in the nervous system. Nature 450 (7166), 56–62.

504 Los, G. V., Encell, L. P., McDougall, M. G., Hartzell, D. D., Karassina, N., Zimprich,
505 C., Wood, M. G., Learish, R., Ohana, R. F., Urh, M., Simpson, D., Mendez, J.,
506 Zimmerman, K., Otto, P., Vidugiris, G., Zhu, J., Darzins, A., Klaubert, D. H.,
507 Bulleit, R. F., Wood, K. V., Jun 2008. Halotag: a novel protein labeling technology
508 for cell imaging and protein analysis. ACS Chem Biol 3 (6), 373–82.

509 Nicolaï, L. J. J., Ramaekers, A., Raemaekers, T., Drozdzecki, A., Mauss, A. S.,
510 Yan, J., Landgraf, M., Annaert, W., Hassan, B. A., Nov 2010. Genetically encoded
511 dendritic marker sheds light on neuronal connectivity in drosophila. Proc Natl Acad
512 Sci U S A 107 (47), 20553–8.

513 Ostrovsky, A., Cachero, S., Jefferis, G., Apr 2013. Clonal analysis of olfaction in
514 drosophila: immunochemistry and imaging of fly brains. Cold Spring Harb Protoc
515 2013 (4), 342–6.

516 Pfeiffer, B. D., Truman, J. W., Rubin, G. M., Apr 2012. Using translational enhancers
517 to increase transgene expression in drosophila. Proc Natl Acad Sci U S A 109 (17),
518 6626–31.

519 Pitman, J. L., Huetteroth, W., Burke, C. J., Krashes, M. J., Lai, S.-L., Lee, T.,
520 Waddell, S., May 2011. A pair of inhibitory neurons are required to sustain labile
521 memory in the drosophila mushroom body. Curr Biol 21 (10), 855–61.

522 Potter, C. J., Tasic, B., Russler, E. V., Liang, L., Luo, L., Apr 2010. The q system:
523 a repressible binary system for transgene expression, lineage tracing, and mosaic
524 analysis. Cell 141 (3), 536–48.

525 Riedl, J., Crevenna, A. H., Kessenbrock, K., Yu, J. H., Neukirchen, D., Bista, M.,
526 Bradke, F., Jenne, D., Holak, T. A., Werb, Z., Sixt, M., Wedlich-Soldner, R., Jul
527 2008. Lifeact: a versatile marker to visualize f-actin. Nat Methods 5 (7), 605–7.

528 Saina, M., Benton, R., 2013. Visualizing olfactory receptor expression and localization
529 in drosophila. Methods Mol Biol 1003, 211–28.

530 Schindelin, J., Arganda-Carreras, I., Frise, E., Kaynig, V., Longair, M., Pietzsch, T.,
531 Preibisch, S., Rueden, C., Saalfeld, S., Schmid, B., Tinevez, J.-Y., White, D. J.,
532 Hartenstein, V., Eliceiri, K., Tomancak, P., Cardona, A., Jun 2012. Fiji: an open-
533 source platform for biological-image analysis. Nat Methods 9 (7), 676–82.

534 Shearin, H. K., Macdonald, I. S., Spector, L. P., Stowers, R. S., Apr 2014. Hexameric
535 gfp and mcherry reporters for the drosophila gal4, q, and lexa transcription systems.
536 Genetics 196 (4), 951–60.

Silbering, A. F., Rytz, R., Grosjean, Y., Abuin, L., Ramdya, P., Jefferis, G. S. X. E., Benton, R., Sep 2011. Complementary function and integrated wiring of the evolutionarily distinct drosophila olfactory subsystems. J Neurosci 31 (38), 13357–75.

Stockinger, P., Kvitsiani, D., Rotkopf, S., Tirián, L., Dickson, B. J., Jun 2005. Neural circuitry that governs *drosophila* male courtship behavior. Cell 121 (5), 795–807.

Team, R. C., 2016. R: A language and environment for statistical computing. URL `https://www.R-project.org/`

Vistain, L. F., Rotz, M. W., Rathore, R., Preslar, A. T., Meade, T. J., Jan 2016. Targeted delivery of gold nanoparticle contrast agents for reporting gene detection by magnetic resonance imaging. Chem Commun (Camb) 52 (1), 160–3.

Viswanathan, S., Williams, M. E., Bloss, E. B., Stasevich, T. J., Speer, C. M., Nern, A., Pfeiffer, B. D., Hooks, B. M., Li, W.-P., English, B. P., Tian, T., Henry, G. L., Macklin, J. J., Patel, R., Gerfen, C. R., Zhuang, X., Wang, Y., Rubin, G. M., Looger, L. L., Jun 2015. High-performance probes for light and electron microscopy. Nat Methods 12 (6), 568–76.

Vosshall, L. B., Wong, A. M., Axel, R., Jul 2000. An olfactory sensory map in the fly brain. Cell 102 (2), 147–59.

Yang, G., de Castro Reis, F., Sundukova, M., Pimpinella, S., Asaro, A., Castaldi, L., Batti, L., Bilbao, D., Reymond, L., Johnsson, K., Heppenstall, P. A., Feb 2015. Genetic targeting of chemical indicators in vivo. Nat Methods 12 (2), 137–9.

8 Supplemental Information

8.1 Materials and Methods

Labeling of tissues was performed as follows.

8.1.1 Triple labeling of Chemical Brainbow Drosophila Brains

We made a double cassette reporter by combing both Brainbow insertions with hs-Bxb1 and *fruitless*-Gal4; a knock in insertion of Gal4 into the P1 promoter of the Fru locus (Stockinger et al., 2005). First we screened several hs-Bxb1 insertions and identified one that produces minimal background activation of the reporters at 25° (that is the line that gave fewest labelled cells with no heat shock). Next, newly hatched larvae were heat-shocked for 10 minutes at 37° and allowed to develop into adults. Flies were then processed as follows:

- All steps were carried out at room temperature unless stated differently.
- Brains were dissected in ice-cold 0.1 M phosphate buffer (PB: 0.032 M NaH_2PO_4, 0.068 M NaH_2PO_4).
- Fixed in 4 % paraformaldehyde (PFA) (in 0.1 M PB) for 30 min in a glass-well plate on an orbital shaker
- Transferred to 1.5 ml tube
- Permeabilized by incubation in 1 ml of PBS-T (phosphate buffered saline + 0.3 % Triton X-100) (2 x 15 min) on rotating wheel
- Incubated with SNAP-Cell 647-SiR (NEB: S9102S) substrate at a final concentration of 1 μM in PBS on rotating wheel for 30 min

- Added CLIP-Surface 488 (NEB: S9232S) and HaloTag TMR (Promega: G8252) at a final concentration of 1 μM to the tube with brains/SNAP-Cell 647-SiR solution
- Incubated on rotating wheel for a further 30 mins
- Washed with PBS-T (2 × 15 min)
- PBS-T was removed as completely as possible and 100 μl of Vectashield (or other) mounting medium added. We observed that subsequently transferring brains into a fresh 100 μl aliquot of Vectashield results in more homogeneous signal along the z axis of the image
- After labeling brains were then mounted on charged slides and imaged

8.1.2 Chemical labeling of Drosophila Antennal Segments

- All steps were carried out at room temperature unless stated differently.
- Antennae were harvested in liquid nitrogen Saina and Benton (2013)
- Fixed in 4% PFA, 3% Triton, 1xPBS (180 min)
- Washed in 3% Triton, 1xPBS (2 x 5 min)
- Washed in 0.1% Triton, 1xPBS (2 x 5 min)
- Incubated in 5 μM Halo-SIR (10 min)
- Washed in 0.1% Triton, 1xPBS (2 x 10min)
- Washed in 0.1% Triton, 1xPBS (2 x 5min)
- After labeling antennae were mounted in Vectashield and imaged

8.1.3 Chemical and Antibody co-labeling Drosophila Antennal Segments

- All steps were carried out at room temperature unless stated differently.
- Antennae were harvested in liquid nitrogen
- Fixed in 4% PFA, 3% Triton, 1xPBS (180 min)
- Washed in 3% Triton, 1xPBS (2 x 10min)
- Washed in 0.1% Triton, 1xPBS (2 x 10min)
- Incubated in 5 μM Halo-SIR (10 min)
- Washed in 0.1% Triton, 1xPBS (2 x 10min)
- Blocked in 5% goat serum, 0.1%Triton, 1xPBS (60 min)
- Incubated with primary antibody in in 5% goat serum, 0.1%Triton, 1xPBS (overnight at 4°)
- Washed in 0.1% Triton, 1xPBS (6 x 15min)
- Blocked in 5% goat serum, 0.1%Triton, 1xPBS (60 min)
- Incubated with secondary antibody in in 5% goat serum, 0.1%Triton, 1xPBS (overnight at 4°)
- Washed in 0.1% Triton, 1xPBS (6 x 15min)
- After labeling antennae were mounted in Vectashield and imaged

8.2 Tables

Tag	Promoter	Insertion site	Conditional	Transgene	Figure
CLIP	UAS	VK00005	-	UAS-myr::4xCLIPf	1, S1
		attP40	-	UAS-myr::4xCLIPf	1, S1
	LexAop2	VK00005	-	LexAop2-myr::4xCLIPf	S2
		attP40	-	LexAop2-myr::4xCLIPf	1
SNAP	UAS	VK00005	-	UAS-myr::4xSNAPf	1, S2
		attP40	-	UAS-myr::4xSNAPf	1, S2
	LexAop2	VK00005	-	LexAop2-myr::4xSNAPf	S2
		attP40	-	LexAop2-myr::4xSNAPf	1
	UAS	VK00005	yes	UAS-myr::>BxbSTOP>-4xSNAPf	-
	LexAop2	VK00018	yes	LexAop2-myr::>BxbSTOP>-4xSNAPf	4
Halo	UAS	attP40	-	UAS-Halo7::CAAX	2
		attP40	-	UAS-3xHalo7::CAAX	2,3
		attP40	-	UAS-7xHalo7::CAAX	2
		attP40	-	UAS-Syt::Halo7	5
		attP40	-	UAS-Syt::3xHalo7	5
		attP40	-	UAS-Syt::7xHalo7	5
		attP40	-	UAS-LA-Halo2	5
Bxb1	heat shock	attP18	-	HeatShock-Bxb1	-
	heat shock	attP40	-	HeatShock-Bxb1	-
	heat shock	P element	-	HeatShock-Bxb1	4
	UAS	VK00027	yes	UAS->FlpSTOP>Bxb1	-
	UAS	VK00027	-	UAS->Bxb1	4
SNAPf CLIPf Halo	UAS	attP2	yes	UAS-ChemicalBrainbow	-
		VK00005	yes	UAS-ChemicalBrainbow	-
		attP2, VK00005	yes	UAS-2xChemicalBrainbow	4

Table S1: **Transgenic flies generated in this study**

Figure	Genotype in figure	Full Genotype
1b	Mz19-Gal4 > UAS-CD4::CLIFf, 2nd chr.	; Mz19-Gal4 / UAS-CD4::CLIPf ; + / Ki
1b	Mz19-Gal4 > UAS-myr::4xCLIPf, attP40	; MZ19-Gal4 / UAS-myr::4xCLIPf in attP40 ;
1b	Mz19-Gal4 > UAS-myr::4xCLIPf, VK00005	; Mz19-Gal4 / CyO;UAS-myr::4xCLIPf in VK00005 / +
1b	Mz19-Gal4 > UAS-myr::SNAPf, attP40	; MZ19-Gal4 / UAS-myr::SNAPf in attP40-5 ; + / Ki
1b	Mz19-Gal4 > UAS-myr::4xSNAPf, attP40	; MZ19-Gal4 / UAS-myr::4xSNAPf in attP40 ; + / MKRS
1b	Mz19-Gal4 > UAS-myr::4xSNAPf, VK00005	; MZ19-Gal4 / CyO;UAS-myr::4xSNAPf in VK00005 / +
1c	GH146-LexA > LexAop2-myr::4xCLIPf, attP40	hsFLP* ; GH146-LexA / LexAop2-myr::4xCLIPf in attP40 ; MB247-Gal4*,QUAS-mtdTomato*/MKRS
1c	GH146-LexA > LexAop2-myr::4xSNAPf, attP40	hsFLP* ; GH146-LexA / LexAop2-myr::4xSNAPf in attP40 ; MB247-Gal4*, QUAS-mtdTomato*/MKRS
1d	Mz19-Gal4 > UAS-myr::4xSNAPf, LexAop2-myr::4xCLIPf	; MZ19-Gal4 / LexAop2-myr::4xCLIPf in attP40 ; OrcoLexAVP16 / UAS-myr::4xSNAPf in VK00005
2b	Mz19-Gal4 > UAS-myr::Halo2, attP40	; MZ19-Gal4, UAS-myr::Halo2 in attP40/CyO ; TM6B / +
2b	Mz19-Gal4 > UAS-Halo7::CAAX, attP40	; MZ19-Gal4 / UAS-Halo7::CAAX in attP40 ;
2b	Mz19-Gal4 > UAS-3xHalo7::CAAX, attP40	; MZ19-Gal4 / UAS-3xHalo7::CAAX in attP40 ;
2b	Mz19-Gal4 > UAS-7xHalo7::CAAX, attP40	; MZ19-Gal4 / UAS-7xHalo7::CAAX in attP40 ;
3a	IR84a-Gal4 > UAS-mCD8::GFP	; UAS-mCD8::GFP ; IR84a-Gal4
3a	IR84a-Gal4 > UAS-myr::4xSNAPf	; UAS-myr::4xSNAPf in attP40 ; IR84a-Gal4
3a, b	IR84a-Gal4 > UAS-3xHalo7::CAAX	; UAS-3xHalo7::CAAX in attP40 ; IR84a-Gal4
4c.i	MB247-Gal4	LexAop2-mCD8::GFP*, UAS-mCD8::RFP/+ ; ; MB247-Gal4 / +
4c.ii	MB247-Gal4 ⋂ nSyb-LexA	; LexAop2-myr::>HA-BxbSTOP>4xSNAPf / nSyb-LexAP65 ; UAS>Bxb1 / MB247-Gal4, QUAS-mtdTomato*
4c.iii	Mz19-Gal4	; MZ19-Gal4 / UAS-myr::4xCLIPf in attP40 ;
4c.iv	Mz19-Gal4 ⋂ nSyb-LexA	; nSyb-LexAP65 LexAop2-myr::>HA-BxbSTOP>4xSNAPf / MZ19-Gal4 ; UAS>Bxb1 / +

Figure	Genotype in figure	Full Genotype
4c.v	Mz19-Gal4 ⋂ MB247-LexA	; Mz19-Gal4 / LexAop2-myr::>HA-BxbSTOP>4xSNAPf ; MB247-LexA / UAS-Bxb1
4d	Fru-Gal4 > 2 x Brainbow cassettes	; hsBxb1 / CyO ; Fru-Gal4 / UAS-myr::>HA-BxbSTOP>SNAPf>CLIPf>Halo2 in attP2, UAS-myr::>HA-BxbSTOP>SNAPf>CLIPf>Halo2 in VK00005
5a	Mz19-Gal4 > UAS-Syt::Halo7	Mz19Gal4 / UAS-Syt::Halo7 in attP40
5a	Mz19-Gal4 > UAS-3xSyt::Halo7	Mz19Gal4 / UAS-3xSyt::Halo7 in attP40
5a	Mz19-Gal4 > UAS-7xSyt::Halo7	Mz19Gal4 / UAS-7xSyt::Halo7 in attP40
5b	BG57-Gal4 > UAS-LA::Halo2	UAS-Dicer2 ; UAS-LA::Halo2 in attP40 / + ; BG57Gal4 / +
S1a	Mz19-Gal4 > UAS-CD4::CLIPf on 2nd	; Mz19-Gal4 / UAS-CD4::CLIPf ;
S1a	50A02-Gal4 > UAS-CD4::CLIPf on 2nd	; UAS-CD4::CLIPf / + ; 50A02-Gal4 / +
S1a	54F05-Gal4 > UAS-CD4::CLIPf on 2nd	; UAS-CD4::CLIPf / + ; 54F05-Gal4 / +
S1a	59F02-Gal4 > UAS-CD4::CLIPf on 2nd	; UAS-CD4::CLIPf / + ; 59F02-Gal4 / +
S1a	Mz19-Gal4 > UAS-CD4::CLIPf on 3rd	; Mz19-Gal4 / + ; UAS-CD4::CLIPf / + ;
S1a	50A02-Gal4 > UAS-CD4::CLIPf on 3rd	; ; UAS-CD4::CLIPf / 50A02-Gal4
S1a	54F05-Gal4 > UAS-CD4::CLIPf on 3rd	; ; UAS-CD4::CLIPf / 54F05-Gal4
S1a	59F02-Gal4 > UAS-CD4::CLIPf on 3rd	; ; UAS-CD4::CLIPf / 59F02-Gal4
S1a	50A02-Gal4 > UAS-mCD8::GFP	50A02-Gal4 / UAS-IVS-mCD8::GFP in attP2
S1a	54F05-Gal4 > UAS-mCD8::GFP	54F05-Gal4 / UAS-IVS-mCD8::GFP in attP2
S1a	59F02-Gal4 > UAS-mCD8::GFP	59F02-Gal4 / UAS-IVS-mCD8::GFP in attP2
S1b	Mz19-Gal4 > UAS-myr::4xCLIPf in attP40	; Mz19-Gal4 / UAS-myr::4xCLIPf in attP40 ;
S1b	50A02-Gal4 > UAS-myr::4xCLIPf in attP40	; UAS-myr::4xCLIPf in attP40 / + ; 50A02-Gal4 / +
S1b	54F05-Gal4 > UAS-myr::4xCLIPf in attP40	; UAS-myr::4xCLIPf in attP40 / + ; 54F05-Gal4 / +
S1b	59F02-Gal4 > UAS-myr::4xCLIPf in attP40	; UAS-myr::4xCLIPf in attP40 / + ; 59F02-Gal4 / +
S1b	Mz19-Gal4 > UAS-myr::4xCLIPf in VK00005	; Mz19-Gal4 / + ; UAS-myr::4xCLIPf in VK00005 / +
S1b	50A02-Gal4 > UAS-myr::4xCLIPf in VK00005	; ; UAS-myr::4xCLIPf in VK00005 / 50A02-Gal4
S1b	54F05-Gal4 > UAS-myr::4xCLIPf in VK00005	; ; UAS-myr::4xCLIPf in VK00005 / 54F05-Gal4
S1b	59F02-Gal4 > UAS-myr::4xCLIPf in VK00005	; ; UAS-myr::4xCLIPf in VK00005 / 59F02-Gal4
S1b	50A02-Gal4 > UAS-mCD8::GFP	; ; 50A02-Gal4 / UAS-IVS-mCD8::GFP in attP2

Figure	Genotype in figure	Full Genotype
S1b	54F05-Gal4 > UAS-mCD8::GFP	; ; 54F05-Gal4 / UAS-IVS-mCD8::GFP in attP2
S1b	59F02-Gal4 > UAS-mCD8::GFP	; ; 59F02-Gal4 / UAS-IVS-mCD8::GFP in attP2
S2a	Mz19-Gal4 > UAS-myr::4xSNAPf in attP40	; Mz19-Gal4 / UAS-myr::4xSNAPf in attP40 ;
S2a	54F05-Gal4 > UAS-myr::4xSNAPf in attP40	; UAS-myr::4xSNAPf in attP40 / + ; 54F05-Gal4 / +
S2a	59F02-Gal4 > UAS-myr::4xSNAPf in attP40	; UAS-myr::4xSNAPf in attP40 / + ; 59F02-Gal4 / +
S2a	54F05-Gal4 > UAS-mCD8::GFP	; ; 54F05-Gal4 / UAS-IVS-mCD8::GFP in attP2
S2a	59F02-Gal4 > UAS-mCD8::GFP	; ; 59F02-Gal4 / UAS-IVS-mCD8::GFP in attP2
S2b	Mz19-Gal4 > UAS-myr::4xSNAPf in attP2	; Mz19-Gal4 / + ; UAS-myr::4xSNAPf in attP2 / + ;
S2b	54F05-Gal4 > UAS-myr::4xSNAPf in attP2	; ; 54F05-Gal4 / UAS-myr::4xSNAPf in attP2
S2b	59F02-Gal4 > UAS-myr::4xSNAPf in attP2	; ; 59F02-Gal4 / UAS-myr::4xSNAPf in attP2
S2b	54F05-Gal4 > UAS-mCD8::GFP	; ; 54F05-Gal4 / UAS-IVS-mCD8::GFP in attP2
S2b	59F02-Gal4 > UAS-mCD8::GFP	; ; 59F02-Gal4 / UAS-IVS-mCD8::GFP in attP2
S2c	GH146-LexA > LexAop2-myr::4xCLIPf in VK00005	GH146-LexA / CyO ; LexAop2-myr::4xCLIPf in VK00005 / +
S2c	GH146-LexA > LexAop2-myr::4xSNAPf in VK00005	GH146-LexA / CyO ; LexAop2-myr::4xSNAPf in VK00005 / +
S3a	OR22a-Gal4 > UAS-mCD8::GFP	; OR22a-Gal4 / UAS-mCD8::GFP ;
S3a	OR22a-Gal4 > ; OR22a-Gal4 / UAS-mCD8::GFP ;	; OR22a-Gal4 / ; OR22a-Gal4 / UAS-mCD8::GFP in attP40 ;

Table S2: **Genotypes of flies used in each figure.** Transgenes marked with an * are not required nor have an effect on the experiment.

8.3 Figures

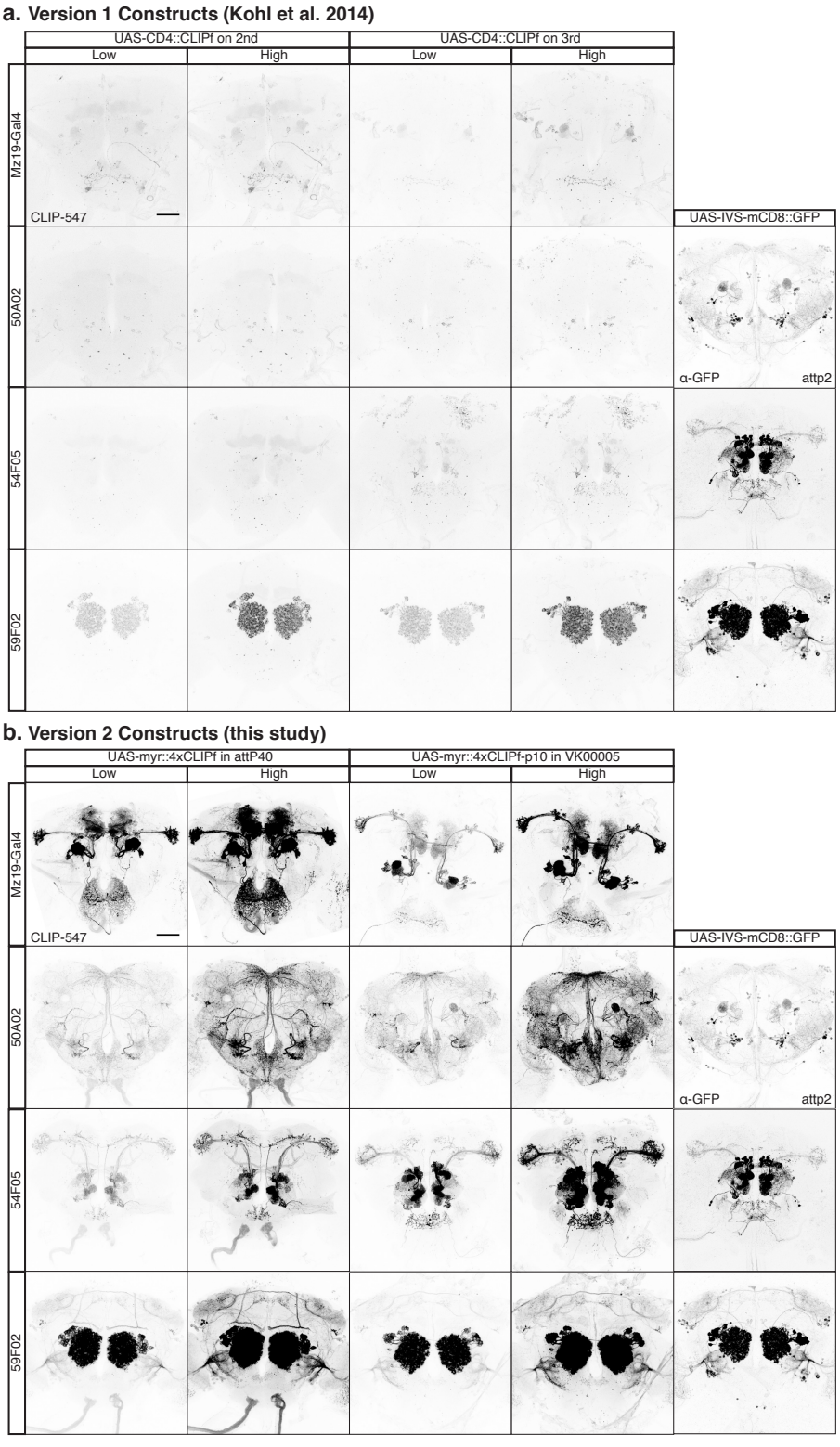

Figure S1: Figure legend on next page

Figure S1: **Labeling Gal4 drivers with old and new CLIPf reporters.** (**a**) Comparison of UAS-CD4::CLIPf, on 2nd and 3rd chromosomes from Kohl et al. (2014), labeling neurons in the Mz19-Gal4, GMR-50A02-Gal4, GMR-59F02-Gal4 and GMR-54F05-Gal4 expression patterns. The right most panels show the labeling of GMR-50A02-Gal4, GMR-59F02-Gal4 and GMR-54F05-Gal4 neurons using UAS-IVS-mCD8::GFP in attP2. (**b**) Comparison of UAS-myr::4xCLIPf, in attP40 and VK00005, labeling neurons in the Mz19-Gal4, GMR-50A02-Gal4, GMR-59F02-Gal4 and GMR-54F05-Gal4 expression patterns. The right most panels again show the labeling of GMR-50A02-Gal4, GMR-59F02-Gal4 and GMR-54F05-Gal4 neurons using UAS-IVS-mCD8::GFP in attP2. All images of chemical tagging reporters taking using the same confocal settings which achieved non-saturated images with the new transgenes. Right-most panels showing GFP staining are reproduced from http://flweb.janelia.org/cgi-bin/flew.cgi and were published in Jenett et al. (2012). All scale bars are 50 μm.

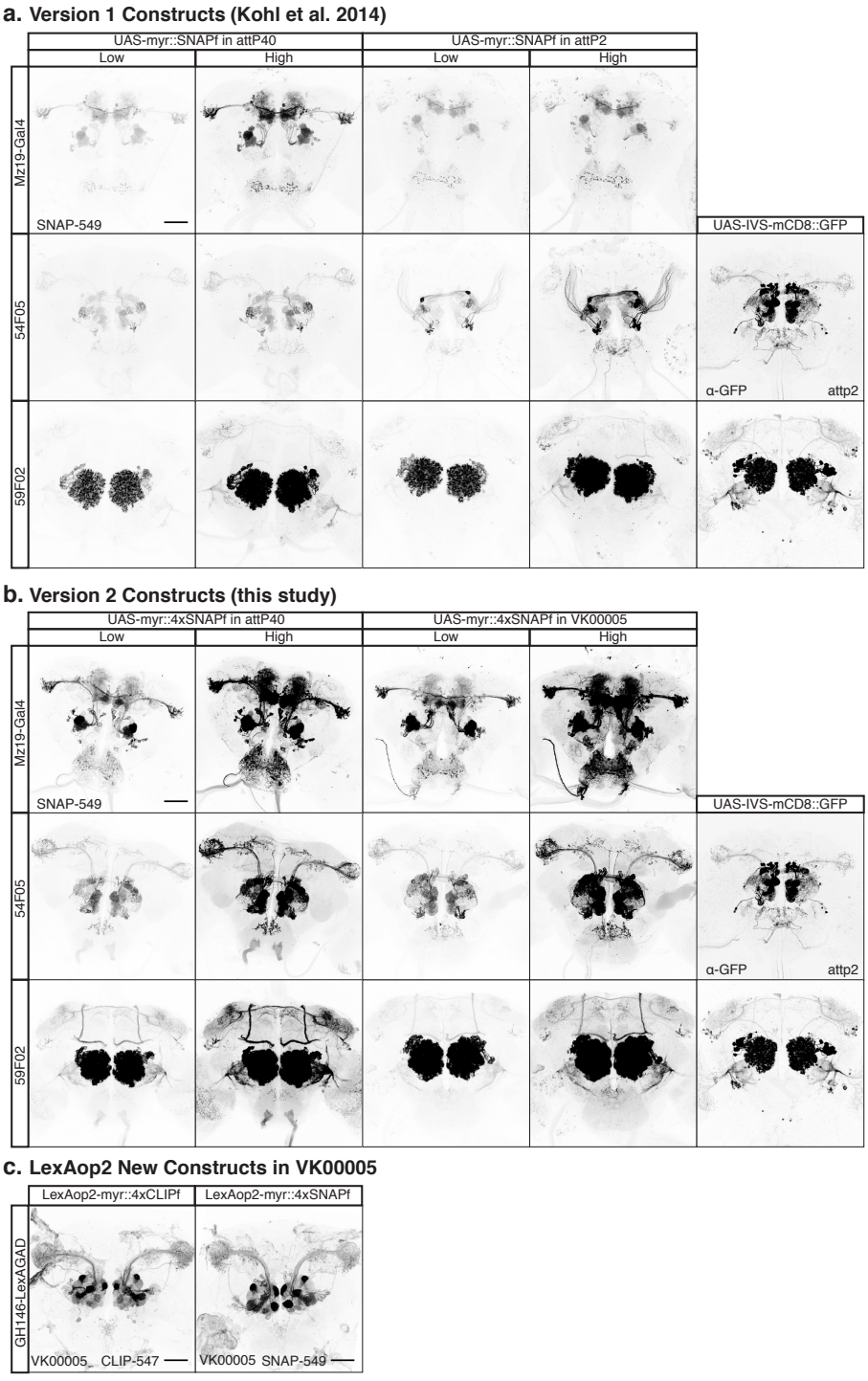

Figure S2: Figure legend on next page

Figure S2: **Labeling of Gal4 drivers with old and new SNAPf reporters.** (**a**) Comparison of version UAS-myr::SNAPf, in attP40 and attP2 from Kohl et al. (2014), labeling neurons in the Mz19-Gal4, GMR-59F02-Gal4 and GMR-54F05-Gal4 expression patterns. The right most panels show the labeling of GMR-59F02-Gal4 and GMR-54F05-Gal4 neurons using UAS-IVS-mCD8::GFP in attP2. (**b**) Comparison of UAS-myr::4xSNAPf, in attP40 and VK00005, labeling neurons in the Mz19-Gal4, GMR-59F02-Gal4 and GMR-54F05-Gal4 expression patterns. The right most panels again show the labeling of GMR-59F02-Gal4 and GMR-54F05-Gal4 neurons using UAS-IVS-mCD8::GFP in attP2. All images of chemical tagging reporters were aquired using the same confocal settings which achieved non-saturated images with the new transgenes. Right-most panels showing GFP staining are reproduced from http://flweb.janelia.org/cgi-bin/flew.cgi and were published in Jenett et al. (2012). All scale bars are 50 µm.

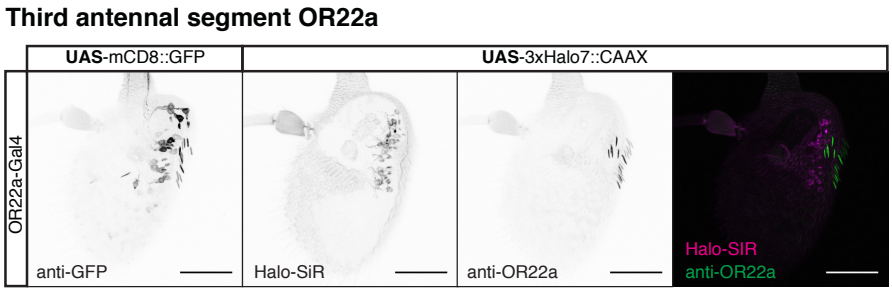

Figure S3: **Combining chemical labeling and antibody staining in the antennae.** Left panel shows staining of mCD8::GFP in Olfactory Receptor 22a expressing sensory neurons (OR22a). Next three panels show chemical labeling of cell membranes and antibody staining of the OR22a receptor. All panels partial projections of confocal stacks that exclude the cuticle. All inset images are the corresponding confocal full projections. All scale bars are 50 µm.

HeatShock-Bxb1-SV40

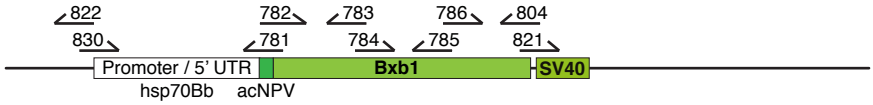

Primer	Sequence	Template
821	aatgagctaaggtctggtgttctagaggatctttgtgaaggaac	pJFRC161
822	gagcttaagactggccgtcgacctgcaggcatgcaagc	
830	cgacggccagtcttaagctcctagaatcccaaaacaaactggttattg	pCASPER-hs
781	ggctcgcattttgttatataatttgtaatttattcagagttctcttcttgtattcaat	
782	aattacaaattatataacaaaatgcgagccctggtcgtcatccgtttgtcccgtgtcac	Bxb1 gene synthesis block 1
783	agacgccactctccatccaca	
784	tgtggatggagagtggcgtct	Bxb1 gene synthesis block 2
785	gcttcgggaatcccatggaa	
786	ttccatgggattcccgaagc	Bxb1 gene synthesis block 3
804	acaccagaccttagctcattccggtgtgcaaacgctcgaccacgctgcccag	

Figure S4: **HeatShock-Bxb1-SV40.**

UAS-myr::>HA-BxbSTOP>SNAPf>CLIPf-p10

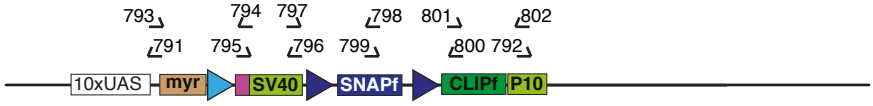

Primer	Sequence	Template
791	cttcttggcagatttcagtagttgcagttg	pJFRC81
792	caaatcaattgttttataatattcgtacgattctttg	
793	caactgcaactactgaaatctgcc	acNPV-myr::attP-HA gene synthesis block
794	cttgatatcgaattcttaagcgtaatctgg	
795	ccagattacgcttaagaattcgatatcaag	QUAS-mtdTomato
796	tgctttatttgtgaaatttgtgatgctattg	
797	caatagcatcacaaatttcacaaataaagca	SV40 UTR-attb-SNAPf gene synthesis block
798	cagcgaggtggctgtagctgatgacctctcc	
799	ggagaggtcatcagctacagccacctcgctg	SNAPf-attb-CLIPf gene synthesis block
800	ctggtggaagtaagcgttcaaccaag	
801	cttggttgaacgcttacttccaccag	CLIPf-p10 gene synthesis block
802	caaagaatcgtacgaatattataaaacaat	

UAS-myr::>HA-BxbSTOP>SNAPf-p10>CLIPf-p10

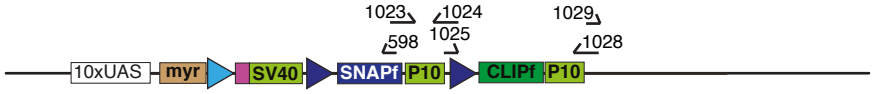

Primer	Sequence	Template
598	ttaacccagcccaggcttgc	UAS-myr::>HA-BxbSTOP> SNAPf>CLIPf-p10
1029	ttgaagacgaaagggcctc	
1023	caagcctgggctgggttaaatgaatcgtttttaaaataacaaatcaattg	UAS-myr::>HA-BxbSTOP> SNAPf>CLIPf-p10
1024	gacaagccgaacctacctttgttaactcgaatcgctatccaagc	
1025	aaaaggtaggttcggcttgtc	UAS-myr::>HA-BxbSTOP> SNAPf>CLIPf-p10
1028	gaggccctttcgtcttcaagttaactcgaatcgctatccaag	

UAS-myr::>HA-BxbSTOP>SNAPf>CLIPf>Halo2-p10

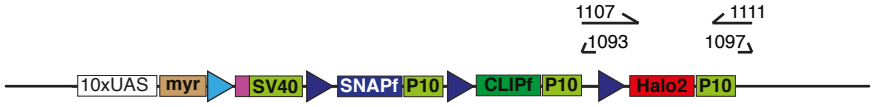

Primer	Sequence	Template
1093	cgaggccctttcgtcttcaag	UAS-myr::>HA-BxbSTOP> SNAPf-p10>CLIPf-p10
1097	ggttaatgtcatgataataatggtttcttag	
1107	gaagacgaaagggcctcgcggcttgtcgacgacggcggtctccgtcgtcag gatcatcttatgggttccgaaatcggtacag	pUAST-myr::Halo2
1111	gaaaccattattatcatgacattaaccgttaactcgaatcgctatccaag	

Figure S5: **UAS-myr::>HA-BxbSTOP>SNAPf>CLIPf>Halo2**

UAS-myr::4xCLIPf

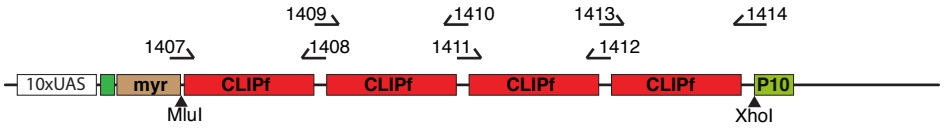

Primer	Sequence	Template
-	Double digest with MluI and XhoI enzymes to generate sticky ends.	UAS-myr::>HA-BxbSTOP> SNAPf-p10>CLIPf-p10>Halo2-p10
1407	gacatcatcagaccacgcgtgatggataaggattgcgagatgaag	UAS-myr::>HA-BxbSTOP> SNAPf-p10>CLIPf-p10>Halo2-p10
1408	tgtactaccgcttacgcttcccaagccgggctttcc	
1409	agcgtaagcggtagtacaatggataaggattgcgagatgaag	UAS-myr::>HA-BxbSTOP> SNAPf-p10>CLIPf-p10>Halo2-p10
1410	ggtactgctaccgcttactcccaagccgggctttcc	
1411	ggagtaagcggtagcagtaccatggataaggattgcgagatgaag	UAS-myr::>HA-BxbSTOP> SNAPf-p10>CLIPf-p10>Halo2-p10
1412	cgtgctactactaccaaccgatcccaagccgggctttcc	
1413	tcggttggtagtagtagcacgatggataaggattgcgagatgaag	UAS-myr::>HA-BxbSTOP> SNAPf-p10>CLIPf-p10>Halo2-p10
1414	gttattttaaaaacgattcattctagattaactagtctcgagtcactatccca agccgggctttcc	

Figure S6: **UAS-myr::4xCLIPf**

UAS-myr::4xSNAPf

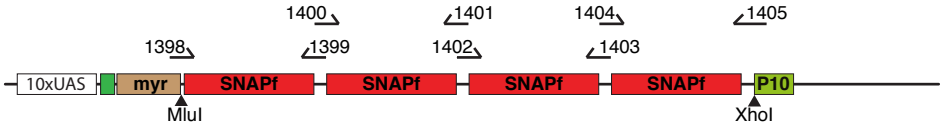

Primer	Sequence	Template
	Double digest with MluI and XhoI enzymes to generate sticky ends.	UAS-myr::>HA-BxbSTOP> SNAPf-p10>CLIPf-p10>Halo2-p10
1398	gacatcatcagaccacgcgtgatggacaaagactgcgaaatgaag	UAS-myr::>HA-BxbSTOP> SNAPf-p10>CLIPf-p10>Halo2-p10
1399	tgtactaccgcttacgctacccagcccaggcttgc	
1400	agcgtaagcggtagtacaatggacaaagactgcgaaatgaag	UAS-myr::>HA-BxbSTOP> SNAPf-p10>CLIPf-p10>Halo2-p10
1401	ggtactgctaccgcttacacccagcccaggcttgc	
1402	ggtgtaagcggtagcagtaccatggacaaagactgcgaaatgaag	UAS-myr::>HA-BxbSTOP> SNAPf-p10>CLIPf-p10>Halo2-p10
1403	cgtgctactactaccaaccgaacccagcccaggcttgc	
1404	tcggttggtagtagtagcacgatggacaaagactgcgaaatgaag	UAS-myr::>HA-BxbSTOP> SNAPf-p10>CLIPf-p10>Halo2-p10
1405	gttattttaaaaacgattcattctagattaactagtctcgagtcactaaccc agcccaggcttgc	

Figure S7: **UAS-myr::4xSNAPf**

LexAop2-myr::4xCLIPf

Primer	Sequence	Template
-	Double digest with NotI and EcoRI enzymes to generate sticky ends.	pJFRC19
1457	ccctaattcttatcctttacttcaggcaattacaaattatataacaaaatggg caacaaatgctgc	UAS-myr::4xCLIPf
1465	gaggccctttcgtcttcaaggttaactcgaatcgctatccaagccag	

Figure S8: **LexAop2-myr::4xCLIPf.** Red restriction enzymes indicate that the site is destroyed during the assembly reaction.

LexAop2-myr::4xSNAPf

Primer	Sequence	Template
-	Double digest with NotI and EcoRI enzymes to generate sticky ends.	pJFRC19
1457	ccctaattcttatcctttacttcaggcaattacaaattatataacaaaatggg caacaaatgctgc	UAS-myr::4xSNAPf
1465	gaggccctttcgtcttcaaggttaactcgaatcgctatccaagccag	

Figure S9: **LexAop2-myr::4xSNAPf**

UAS-myr::>HA-BxbSTOP>4xSNAPf

Primer	Sequence	Template
1399	tgtactaccgcttacgctacccagcccaggcttgc	UAS-myr::>HA-BxbSTOP>SNAPf
1406	tagtgactcgagactagttaatctagaatgaatcg	-p10>CLIPf-p10>Halo2-p10
1400	agcgtaagcggtagtacaatggacaaagactgcgaaatgaag	UAS-myr::>HA-BxbSTOP>SNAPf
1401	ggtactgctaccgcttacacccagcccaggcttgc	-p10>CLIPf-p10>Halo2-p10
1402	ggtgtaagcggtagcagtaccatggacaaagactgcgaaatgaag	UAS-myr::>HA-BxbSTOP>SNAPf-
1403	cgtgctactactaccaaccgaacccagcccaggcttgc	p10>CLIPf-p10>Halo2-p10
1404	tcggttggtagtagtagcacgatggacaaagactgcgaaatgaag	UAS-myr::>HA-BxbSTOP>SNAPf-
1405	gttattttaaaaacgattcattctagattaactagtctcgagtcactaaccca gcccaggcttgc	p10>CLIPf-p10>Halo2-p10

Figure S10: **UAS-myr::>HA-BxbSTOP>4xSNAPf**

LexAop2-myr::>HA-BxbSTOP>4xSNAPf

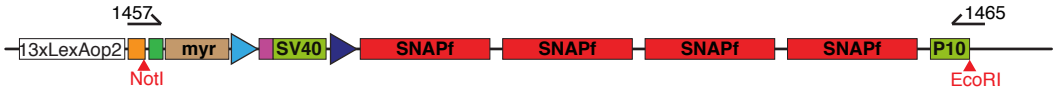

Primer	Sequence	Template
-	Double digest with NotI and EcoRI enzymes to generate sticky ends.	pJFRC19
1457	ccctaattcttatcctttacttcaggcaattacaaattatataacaaaatggg caacaaatgctgc	UAS-myr::>BxbSTOP>4xSNAPf
1465	gaggccctttcgtcttcaaggttaactcgaatcgctatccaagccag	

Figure S11: **LexAop2-myr::>HA-BxbSTOP>4xSNAPf**

HeatShock-Bxb1

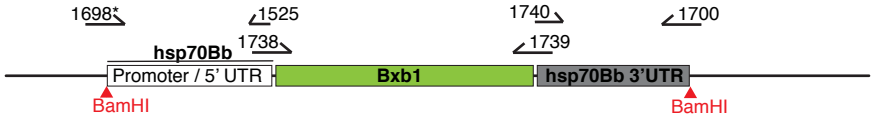

Primer	Sequence	Template
-	Digest with BamHI enzyme to generate sticky ends.	pUAST-TLN-cherry (Nicolaï et al., 2010)
1698	aagcttctgcatctctccgctagaatcccaaaacaaactggttattgtgg	heatshock-Bxb-SV40 3' UTR
1525	tattcagagttctcttcttgtattcaataattac	
1738	gtaattattgaatacaagaagagaactctgaatacaaaatgcgagccctggtcgtc	heatshock-Bxb-SV40 3' UTR
1739	gaactgaataattttctatttggctttagtcttagctcattccggtgtgcaaac	
1740	gactaaagccaaatagaaaattattcagttcc	Fly genomic DNA
1700	catacatactaaggccttctagtggatctaaacgagtttttaagcaaac	

Figure S12: **HeatShock-Bxb1**. Red restriction enzymes indicate that the site is destroyed during the assembly reaction. Part of the sequence for primer 1698* was not found on the cloned construct; the difference being upstream of the functional sequences does not affect its activity.

UAS->FlpSTOP>Bxb1

UAS->Bxb1

Primer	Sequence	Template
1344	gtacaaagtggtgggtaccggatc	pJFRC-MUH-FRT-hsp70Bb-FRT (unpublished)
1337	gccggccgcaactagaactag	
1338	ctagttctagttgcggccggctaagaattcgatatcaagcttatcgataccg	UAS-myr::>HA-BxbSTOP> SNAPf-p10>CLIPf-p10>Halo2-p10
1340	gacgaccagggctcgcattttggaagttcctatactttctagagaataggaa cttcgatccagacatgataagatacattgatgagtttg	
1339	atgcgagccctggtcgtc	heatshock-Bxb-SV40 3' UTR
1345	cggtacccaccactttgtacttagctcattccggtgtgcaaac	

Figure S13: **UAS->FlpSTOP>Bxb1**. UAS->Bxb1 was obtained by activating UAS-FLP on the germ line of males using nanos-Gal4. Flp recombination induces removal of the stop cassette in the germ line and allowed the establishment of a stock.

pJET p1.2-1xHalo7::CAAX

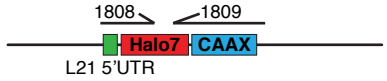

Cloning steps
Syn21-Halo7::CAAX PCR product (see table below) was blunt-end ligated into vector pJET p1.2 (ThermoFisher Scientific).

Primer	Sequence	Template
1808	ttcaggcggccgcaactcctaaaaaaccgccaccatggcagaaatcggtactggc	pHTN-JF920304; Promega Inc.
1809	ccctctagattacataattacacactttgtctttgacttctttttcttcttttac catctttgctcatctcgagactagtagatctgccggaaatttcgagcgtcgaca	

UAS-1xHalo7::CAAX

Cloning steps
- Following sequence verification, pJET p1.2-1xHalo7::CAAX was digested with Not1 and Xba1.
- The Halo7::CAAX fragment was ligated into the Drosophila transformation vector, pJFRC81 using Not1 and Xba1 sites.

Figure S14: **UAS-1xHalo7::CAAX**.

pJET p1.2-1xHalo7

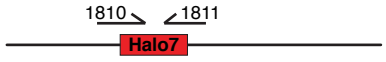

Cloning steps		
Halo7 PCR product (see table below) was blunt-end ligated into vector pJET p1.2 (ThermoFisher Scientific).		
Primer	**Sequence**	**Template**
1810	gggaccggttctagaggatccatggcagaaatcggtactggc	pHTN-JF920304; Promega Inc.
1811	ccctctagattactcgagactagtagatctgccggaaatttcgagcgtcgaca gccagcg	

pJET p1.2-2xHalo7

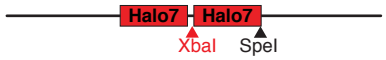

Cloning steps
- Following sequence verification, pJET p1.2-1xHalo7 was digested with with XbaI and SpeI.
- The Halo fragment was re-inserted into pJET p1.2-1xHalo7 digested with SpeI. During this step the XbaI site (red) combines with the SpeI site and gets destroyed while one SpeI site gets retained.

UAS-3xHalo7::CAAX

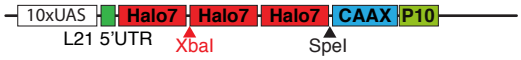

Cloning steps
- pJET p1.2-2xHalo7 was digested with Xba1 and Spe1 and the 2xHalo fragment was purified.
- UAS-1xHalo7::CAAX was treated with SpeI and the 2xHalo fragment ligated. During the cloning the XbaI site gets destroyed and the SpeI site is retained.

Figure S15: **UAS-3xHalo7::CAAX.**

pJET p1.2-4xHalo7

Cloning steps
- Following sequence verification, pJET p1.2-2xHalo7 was digested with with XbaI and SpeI.
- The 2xHalo fragment was re-inserted into pJET p1.2-2xHalo7 digested with SpeI. During this step the XbaI site (red) combines with the SpeI site and gets destroyed while one SpeI site gets retained.

UAS-7xHalo7::CAAX

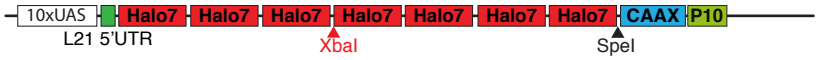

Cloning steps
- pJET p1.2-4xHalo7 was digested with Xba1 and Spe1 and the 4xHalo fragment was purified.
- UAS-3xHalo7::CAAX was treated with SpeI and the 4xHalo fragment ligated. During the cloning the XbaI site gets destroyed and the SpeI site is retained.

Figure S16: **UAS-7xHalo7::CAAX.**

UAS-Synaptotagmin::1xHalo7

Cloning steps
- A previously made Drosophila transformation vector plasmid bearing the Synaptotagmin coding region, pJFRC81-Syt::TMP (unpublished), was digested with Age1 and Xho1.
- The purified pJFRC81-Syt was ligated with a Halo7 fragment from pJET 1.2-Halo7 digested with Age1 and Xho1 to create pJFRC81-Syt::Halo7.

Figure S17: **UAS-Synaptotagmin::1xHalo7**

UAS-Synaptotagmin::3xHalo7

Cloning steps
- pJET p1.2-2xHalo7 was digested with Xba1 and Spe1 and the 2xHalo fragment was purified.
- UAS-Synaptotagmin::Halo was treated with SpeI and the 2xHalo fragment ligated. During the cloning the XbaI site gets destroyed and the SpeI site is retained.

Figure S18: **UAS-Synaptotagmin::3xHalo7**

UAS-Synaptotagmin::7xHalo7

Cloning steps
- pJET p1.2-4xHalo7 was digested with Xba1 and Spe1 and the 4xHalo fragment was purified.
- UAS-Synaptotagmin::3xHalo was treated with SpeI and the 4xHalo fragment ligated. During the cloning the XbaI site gets destroyed and the SpeI site is retained.

Figure S19: **UAS-Synaptotagmin::7xHalo7**

UAS-LifeAct::Halo2

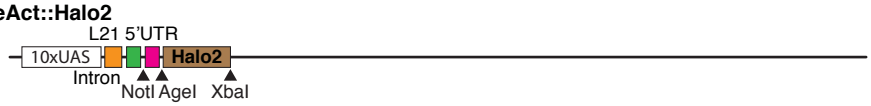

Cloning steps
- pJFRC81-myr::Halo2 Kohl et al. (2014) was digested with Xba1 and Age1 and purified.
- Halo2 fragment was ligated in a previously prepared pJFRC81-LifeAct digested with Xba1 and Age1.

Figure S20: **UAS-LA-Halo2**